

Deep Video Codec Control for Vision Models

Christoph Reich^{1 2 3 4} Biplob Debnath¹ Deep Patel¹ Tim Prangemeier² Daniel Cremers^{3 4}
Srimat Chakradhar¹

Abstract

Standardized lossy video coding is at the core of almost all real-world video processing pipelines. Rate control is used to enable standard codecs to adapt to different network bandwidth conditions or storage constraints. However, standard video codecs (*e.g.*, H.264) and their rate control modules aim to minimize video distortion w.r.t. human quality assessment. We demonstrate empirically that standard-coded videos vastly deteriorate the performance of deep vision models. To overcome the deterioration of vision performance, this paper presents the first end-to-end learnable *deep video codec control* that considers both *bandwidth constraints* and *downstream deep vision performance*, while *adhering to existing standardization*. We demonstrate that our approach better preserves downstream deep vision performance than traditional approaches.

1. Introduction

Video data is a major source of internet traffic (Barnett et al., 2018). A significant and increasing amount of these videos is consumed and analyzed by deep vision models (Hu et al., 2023). Streaming video data over a network or storing the video requires lossy video codecs and rate control to meet dynamic bandwidth and storage constraints, preventing video corruption or frame dropping (Itsumi et al., 2022).

Almost all real-world video processing pipelines utilize standardized video coding, such as H.264 (Wiegand et al., 2003), to ensure interoperability (Lederer, 2019). While deep video codecs have demonstrated promising results and can be optimized for deep vision models, they find minimal to no application in real-world (Lederer, 2019; Wood, 2022). This is due to the lack of standardization (ISO) and limited rate control (*cf.* Table 1) (Zhang et al., 2023).

¹NEC Laboratories America, Inc., USA ²Technical University of Darmstadt, Germany ³Technical University of Munich, Germany ⁴Munich Center for Machine Learning, Germany. Correspondence to: Christoph Reich <c.reich@tum.de>.

Table 1. High-level comparison to existing approaches.

	Optimize vision perf.	Rate control	ISO
Deep video codecs	✓	~	✗
Standard video codecs (<i>e.g.</i> , H.264)	✗	✓	✓
Deep video codec control	✓	✓	✓

Standard video codecs are developed to minimize image distortion w.r.t. human quality assessment (Richardson, 2004). We demonstrate empirically that this is suboptimal for current deep vision models. More specifically, using H.264 coded videos during inference leads to a vast deterioration in downstream vision performance (Otani et al., 2022).

In this paper, we aim to optimize standard video codecs for deep vision models (*e.g.*, a semantic segmentation network) by learning a deep video codec control (Figure 3). For a given video clip \mathbf{V} , we formulate the codec control task as a constrained optimization problem

$$\begin{aligned} \max_{\mathbf{QP}} & M(\text{DNN}(\text{H.264}(\mathbf{V}, C_{\theta}(\mathbf{V}, b)))) \\ \text{s.t. } & \tilde{b} \leq b. \end{aligned} \quad (1)$$

Our lightweight control network C_{θ} consumes both the video clip \mathbf{V} and the (dynamic) target bitrate b to predict high-dimensional codec parameters \mathbf{QP} . We aim to learn a content and bandwidth-aware prediction of \mathbf{QP} , controlling the H.264 coding, such that we maximized the performance of a deep vision model DNN , measured by a task-specific metric M (*e.g.*, accuracy). Additionally, the resulting video bitrate \tilde{b} should not exceed the target bitrate b . To the best of our knowledge, we present the first end-to-end learnable codec control taking vision performance, bandwidth conditions, and existing standardizations into account (*cf.* Table 1). Making our deep video codec control the first standardized approach to support real-world bandwidth conditions as well as deep vision models.

Although approaches for optimizing standard video codecs for vision models within the scope of standardization have been proposed, they entail significant limitations impeding their real-world application (Galteri et al., 2018; Du et al., 2022; Itsumi et al., 2022). First, existing approaches heavily rely on the use of saliency maps and hand-crafted rules (Galteri et al., 2018; Du et al., 2022). However, saliency maps

often fail to express highly relevant regions for deep vision models due to saturating gradients (Sundararajan et al., 2017). Second, existing approaches only consider the preservation of vision performance and do not consider rate control (Galteri et al., 2018; Du et al., 2022; Itsumi et al., 2022). In contrast, our deep video codec control is not limited by the concept of saliency maps, does not rely on hand-crafted rules, and considers both the preservation of downstream vision performance as well as rate control, offering a greater potential for practical application.

Contributions. Motivated by the *potential performance gains* and the *need for standardization*, we make the following contributions: (1) We showcase that downstream deep vision performance vastly deteriorates when standard video coding is employed. (2) We propose the first end-to-end learnable codec control, directly optimizing Equation (1), while maintaining compliance with standardizations. (3) To enable end-to-end learning, we introduce a conditional differentiable surrogate model of a standard codec, allowing gradient propagation through the non-differentiable standard codec w.r.t. high-dimensional codec parameters. We showcase the effectiveness of our deep codec control by controlling H.264 for two classical vision tasks (semantic segmentation and optical flow estimation) and on two datasets (Cityscapes (Cordts et al., 2016) and CamVid (Brosstow et al., 2009)).

2. H.264 and Deep Vision Performance

H.264/AVC performs efficient lossy video compression by exploiting image compression techniques and temporal redundancies (Wiegand et al., 2003). The predictive coding architecture of the H.264 codec utilizes sophisticated hand-crafted transformations to analyze redundancy within videos. A macroblock-wise motion-compensated discrete cosine transform (DCT) followed by quantization and lossless coding is used to archive effective video compression.

Quantization parameter. The H.264 codec allows for a variety of different customizations to the encoding pro-

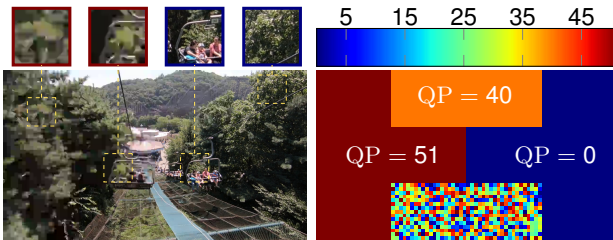


Figure 1. H.264 macroblock-wise encoding example. Effect of different macroblock-wise quantization parameters on the visual quality. Video frame (left) is encoded with QP map (right) as an I-frame. Video data from REDS dataset Nah et al. (2019).

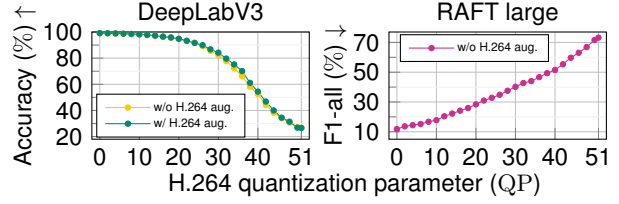


Figure 2. Vision performance vs. compression. Cityscapes segmentation accuracy and optical flow estimation performance, measured by the average endpoint error (AEPE), for different H.264 quantization parameters between the raw clip predictions (pseudo label) and the coded clip predictions. QP is applied uniformly.

cess (Richardson, 2011). The quantization parameter (QP) controls the quantization strength and is the key parameter to control the compression strength. QP ranges from 0 to 51 (integer range), with high values leading to stronger compression. Strong compression reduces bitrate at the cost of video distortion, measured by SSIM (structural similarity index measure) (Wang et al., 2004). Note that, for a given set of codec parameters, the bitrate remains non-trivially dependent on the video content. For example, a video with entirely black frames requires vastly fewer bits than a natural video, while being encoded with the same codec parameters.

Macroblock-wise quantization. H.264 offers support for macroblock-wise quantization, in which regions of the video, in this case, 16×16 frame patches (macroblocks), are compressed with varying QP values. Thus, irrelevant regions can be compressed with a high QP value (strong compression) and relevant regions with a lower QP value (less compression). An example of macroblock-wise coding is given in Figure 1. We employ macroblock-wise quantization to facilitate a fine-grain spatial and temporal control of the video distortion and bitrate (Lampert, 2006).

Group of pictures. The group of pictures (GOP) size further influences the encoding, by controlling which frames are encoded as an I, B, or P-frame. I-frames (intra-coded frames) are only compressed by utilizing spatial redundancies (similar to image coding), whereas B-frames (bidirectional predicted frames) and P-frames (predicted frames) also use information from adjacent frames. In particular, B-frames are compressed by utilizing a previous and a subsequent I- or P-frame. For compressing P-frames only a single previous I- or P-frame is used.

Deep vision performance on H.264 coded videos. We empirically showcase that lossy compressing videos with H.264 can severely deteriorate downstream performance. When uniformly (for all macroblocks) increasing QP, both segmentation accuracy (DeepLabV3 (Chen et al., 2017)) and optical flow estimation (RAFT (Teed & Deng, 2020)) performance decreased, with reference to the prediction obtained

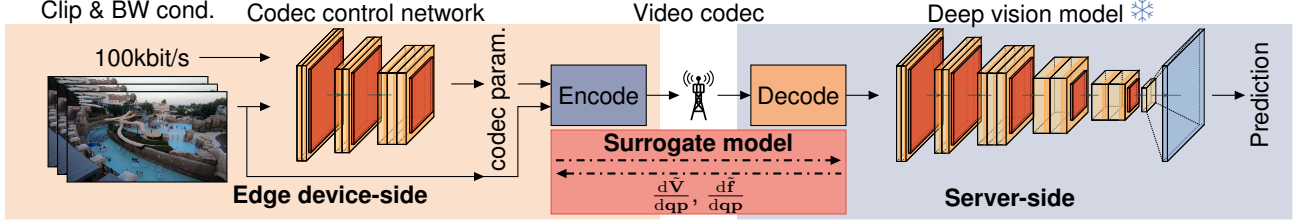


Figure 3. Deep video codec control pipeline. The control network predicts high-dimensional codec parameters for an input clip and a given dynamic network bandwidth (BW) condition. The video clip is encoded using the predicted codec parameters, sent over the network to the server-side, decoded, and analyzed by a deep vision model (e.g., segmentation model). At training, the pre-trained server-side model is fixed and a differentiable surrogate model of the standard codec is used to propagate gradients from the server-side model and the file size prediction to the control network. During inference, the surrogate model is not used. Video frames from Nah et al. (2019).

on the original uncompressed video. Otani et al. (2022) observed the same for action recognition. Using H.264 augmented frames during training cannot help to overcome this issue. We trained a DeepLabV3 model (w/ ResNet-18 (He et al., 2016) backbone) on H.264 coded frames (H.264 aug.). While consuming coded frames during training performance is still highly affected by the compression. Figure 2 visualizes the results of these experiments. We aim to learn the allocation of QP such that downstream performance is better preserved and a target bandwidth is met. Additional experiments and experimental details are in the supplement.

3. Method

Here we introduce our deep video codec control (cf. Figure 3). Before we describe our novel deep video codec control we present our H.264 codec surrogate model. Surrogate modeling the H.264 in a differentiable manner is required to enable our end-to-end codec control training.

3.1. Differentiable H.264 surrogate model

The H.264 video codec is not differentiable due to discreet operations (non-differentiable) and quantizations (gradient zero or undefined). To enable a gradient flow from the vision model and the generated bandwidth to the codec control network we aim to build a conditional differentiable surrogate model of H.264.

We consider H.264 coding (encoding & decoding) as a continuous¹ black-box function mapping the original (raw) video V conditioned on the macroblock-wise quantization parameters QP to the encoded and decoded video \hat{V} as well as the encoded per-frame file size f

$$\begin{aligned} \text{H.264}(V, QP) &= (\hat{V}, f), \quad V, \hat{V} \in \mathbb{R}^{3 \times T \times H \times W}, \\ QP &\in \{0, \dots, 51\}^{T \times H/16 \times W/16}, \quad f \in \mathbb{R}_+^T. \end{aligned} \quad (2)$$

T indicates the number of frames and $H \times W$ the spatial

¹Standard H.264 maps from discreet input to discreet outputs. To enable continuous differentiation we extend the H.264 surrogate mapping to real-valued input and output videos.

dimensions of the RGB video. Other H.264 parameters are considered to be constant. In particular, we consider a GOP of 8 (thus, $T = 8$) and a default preset (Tomar, 2006).

Intuitively, our surrogate model fulfills two tasks during the codec control training (cf. Figure 3). First, it allows our codec control network to consume gradient-based feedback from the downstream model regarding its performance. Second, the codec control network can also get gradient-based feedback w.r.t. the generated and required bandwidth/file size through our differentiable file size prediction.

Surrogate model architecture. Our H.264 surrogate model architecture (cf. Figure 4) is motivated by computational and memory efficiency and encodes inductive biases from the original (non-diff) H.264 coding approach. In general, our surrogate model entails an encoder-decoder architecture with a bottleneck stage (Ronneberger et al., 2015). For computational efficiency, we constrain the encoder and decoder to the frame level. To efficiently learn temporal interactions, we present an aligned convolutional gated recurrent unit (AGRU) for each frame type (I-, P-,

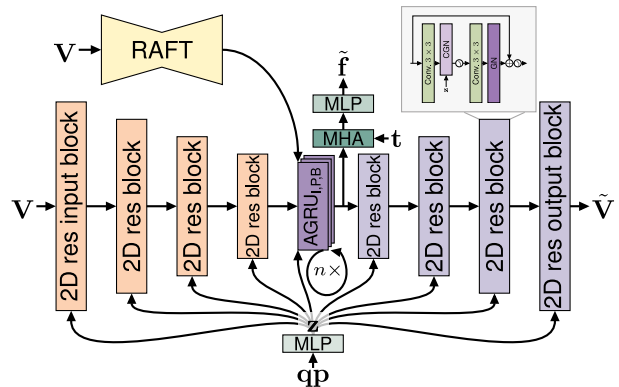


Figure 4. Surrogate model architecture. Our model is composed of a 2D encoder (orange), a 2D decoder (blue), an MHA-based file size head, and three AGRU bottleneck blocks. We use RAFT to compute the optical flows for the AGRU blocks. For embedding the qp we use an MLP. Skip-connections omitted for simplicity.

and B-frame) (Ballas et al., 2016). By using the optical flow prediction of a pre-trained (small) RAFT model (Teed & Deng, 2020), we align adjacent frames used to compress P- and B-frames in each AGRU iteration. Based on the output features of the AGRU we regress the file size on a per-frame level. Our file size head utilizes Multi-Head Attention (Vaswani et al., 2017) to perform cross-attention between learnable query tokens $\mathbf{t} \in \mathbb{R}^{3 \times C_t}$ and the AGRU output features to regress the per-frame file size. We utilize individual tokens for each frame type (I-, P-, and B-frame) and repeat the query tokens for each frame.

To condition both the encoder, decoder, and bottleneck block on QP we use a multilayer perceptron (MLP) to embed QP into a latent vector $\mathbf{z} \in \mathbb{R}^{C_z \times T \times H/16 \times W/16}$. To incorporate \mathbf{z} into the surrogate we used conditional group normalization (CGN) (de Vries et al., 2017). The CGN layer combines a spatial feature transform layer (Wang et al., 2018) followed by a group normalization layer (Wu & He, 2018) (w/o learnable parameters). Note our surrogate model uses one-hot encoded quantization parameters, denoted as $\mathbf{qp} \in \{0, 1\}^{52 \times T \times H/16 \times W/16}$. This allows us to later formulate the prediction of the integer-valued QP as a classification problem. Our resulting surrogate architecture is fully differentiable w.r.t. both the input video clip \mathbf{V} and \mathbf{qp} .

Aligned convolutional gated recurrent unit. Taking inspiration from the motion-compensated and GOP-based compression performed by H.264 (and other standard codecs) we propose to utilize AGRUs in the bottleneck stage of our surrogate model. Our AGRU aims to approximate H.264 compression in an iterative fashion in latent space. Through an alignment in the latent space temporal interactions between the frame to be compressed and the reference frames are efficiently modeled. In particular, we utilize separate AGRUs for each frame type.

The B-frame AGRU is described by

$$\begin{aligned} \mathbf{Z}_{t+1} &= \sigma(\text{CGN}(\mathbf{C}_{3 \times 3}(\mathbf{H}_t) + \mathbf{C}_{3 \times 3}([\hat{\mathbf{A}}_t, \tilde{\mathbf{A}}_t]), \mathbf{z})) \\ \mathbf{R}_{t+1} &= \sigma(\text{GN}(\mathbf{C}_{1 \times 1}(\mathbf{H}_t) + \mathbf{C}_{1 \times 1}([\hat{\mathbf{A}}_t, \tilde{\mathbf{A}}_t]))) \\ \bar{\mathbf{H}}_{t+1} &= \tanh(\text{GN}(\mathbf{C}_{1 \times 1}(\mathbf{R}_{t+1} \odot \mathbf{H}_t) + \mathbf{C}_{1 \times 1}([\hat{\mathbf{A}}_t, \tilde{\mathbf{A}}_t]))) \\ \mathbf{H}_{t+1} &= (1 - \mathbf{Z}_{t+1}) \odot \mathbf{H}_t + \mathbf{Z}_{t+1} \odot \bar{\mathbf{H}}_{t+1}, \end{aligned} \quad (3)$$

where $\mathbf{C}_{3 \times 3}$ and $\mathbf{C}_{1 \times 1}$ denote a 3×3 and a 1×1 2D convolution, respectively. We do not share parameters between convolutions. \mathbf{H}_t are the latent features of the B-frame. $\hat{\mathbf{A}}_t$ and $\tilde{\mathbf{A}}_t$ are the aligned previous and subsequent frame features used for compression based on the GOP structure. We align the features of the frames used for compression by $\hat{\mathbf{A}}_t = \overleftarrow{w}(\hat{\mathbf{H}}_t, \text{RAFT}(\mathbf{V}_t, \hat{\mathbf{V}}_t))$. We backward warp (\overleftarrow{w}) the unaligned features $\hat{\mathbf{H}}_t$ based on the optical flow between the frame to be compressed \mathbf{V}_i and the reference frame $\hat{\mathbf{V}}_j$, using RAFT. We downsample the optical flow to match the spatial dimension of the latent features. For P-frames, we

utilize one reference frame. In the case of an I-frame we fully omit the conditioning in the AGRU. Note the reference frames for B- and P-frame compression can be obtained by the known GOP structure (Wiegand et al., 2003).

Surrogate model training. In general, we are interested that our surrogate model approximates both the H.264 function ($\hat{\mathbf{V}} \approx \tilde{\mathbf{V}}, \mathbf{f} \approx \tilde{\mathbf{f}}$, cf. Eq. (2)) and provide smooth gradients w.r.t. the quantization parameters ($\frac{d\hat{\mathbf{V}}}{d\mathbf{qp}}, \frac{d\tilde{\mathbf{f}}}{d\mathbf{qp}}$). Based on the control variates theory, the surrogate model can become a low-variance and continuous gradient estimator of Equation (2) if (1) the difference between the output of the surrogate and the true H.264 function is minimized and (2) the two output distributions are maximizing the correlation coefficients ρ (Glynn & Szechtmann, 2002; Grathwohl et al., 2018). We enforce both requirements for $\tilde{\mathbf{V}}$ and $\tilde{\mathbf{f}}$ by minimizing $\mathcal{L}_s = \mathcal{L}_{s_v} + \mathcal{L}_{s_f}$ during training. \mathcal{L}_{s_v} supervises the per-frame file size prediction and is defined as

$$\mathcal{L}_{s_f} = \alpha_{\rho_f} \mathcal{L}_{\rho_f} + \alpha_{L1} \mathcal{L}_{L1}. \quad (4)$$

\mathcal{L}_{ρ_f} is the correlation coefficient loss (Tian et al., 2021) between the true file size \mathbf{f} and the predicted file size $\tilde{\mathbf{f}}$. \mathcal{L}_{L1} is used to minimize the distance between \mathbf{f} and $\tilde{\mathbf{f}}$. Note that we learn $\tilde{\mathbf{f}}$ in \log_{10} -space due to the large range of file sizes.

To learn the prediction of the coded video $\tilde{\mathbf{V}}$ we minimize

$$\mathcal{L}_{s_v} = \alpha_{\rho_v} \mathcal{L}_{\rho_v} + \alpha_{\text{SSIM}} \mathcal{L}_{\text{SSIM}} + \alpha_{\text{FF}} \mathcal{L}_{\text{FF}}. \quad (5)$$

\mathcal{L}_{ρ_f} is the correlation coefficient loss for the coded video prediction. We minimize the distance between $\hat{\mathbf{V}}$ and $\tilde{\mathbf{V}}$ both in pixel space and frequency space. In particular, we use the structural similarity measure (SSIM) loss (Zhao et al., 2016) for minimizing the error in pixel space. Taking inspiration from the frequency-based compression utilized by H.264, we utilize the focal frequency loss (Jiang et al., 2021), minimizing prediction error in the frequency space. α is used to denote the different weighting parameters.

3.2. Deep video codec control

We aim to learn a deep codec control solving our constrained optimization (cf. Equation (1)). In particular, given a video clip and a dynamic target bandwidth our deep codec control should predict high-dimensional codec parameters (QP), such that downstream performance is preserved while staying within the target bandwidth. Our general architecture is depicted in Figure 3. Note, while we demonstrate our general codec control on the task of semantic segmentation and optical flow estimation in this paper, the general training formulation (cf. Equation (6)) is agnostic to the vision task to be performed. The only requirement of our approach is the differentiability of the server-side vision model.

Control network. Our control network (cf. Figure 5) consumes a original video clip \mathbf{V} as well as a target bandwidth

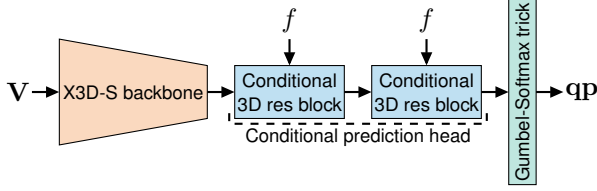


Figure 5. Our control network is composed of a pre-trained X3D-S backbone followed by two conditional 3D residual blocks. The one-hot qp vector is obtained by using the Gumbel-Softmax trick.

f and predicts the macroblock-wise QP. To facilitate the deployment on a standard edge device, such as the NVIDIA Jetson Nano, we use a lightweight architecture. In particular, we utilize X3D-S (Feichtenhofer, 2020) as our control network. To input the bandwidth condition to the network we omit the X3D classification head and use two residual blocks with conditional normalization (de Vries et al., 2017).

Due to the discreet nature of QP (integer-valued), we formulate the QP prediction as a classification. Our control network learns to predict a logit vector over all possible QP values. During end-to-end training, the Gumbel-Softmax trick (Jang et al., 2017) is used to produce a differentiable one-hot qp vector based on the predicted logits. During inference, when used as an input to the original H.264 codec and not to the surrogate, we apply the $\arg \max$ function.

Self-supervised control training. We propose a self-supervised training strategy to train our control network. To utilize end-to-end gradient-based learning we reformulate the constrained optimization problem (cf. Equation (1)) as a continuous optimization task. In particular, our control loss \mathcal{L}_c consists of three terms - the bandwidth loss \mathcal{L}_b , a performance loss \mathcal{L}_p , and a bandwidth regularizer \mathcal{L}_r ,

$$\mathcal{L}_c = \alpha_b \mathcal{L}_b + \alpha_p \mathcal{L}_p + \alpha_r \mathcal{L}_r. \quad (6)$$

where each individual loss is weighted by a separate regularization parameter α .

The bandwidth loss \mathcal{L}_b is used to enforce that the deep codec control satisfies the network bandwidth condition (cf. Equation (1)) and is defined as

$$\mathcal{L}_b = \max(0, \tilde{b} - b(1 - \epsilon_p)), \quad (7)$$

where b is the maximum available bandwidth (bandwidth condition). \tilde{b} denotes the bandwidth prediction computed based on the surrogate model file size prediction \tilde{f} . We convert the per-frame file size (in B) to the bandwidth (in bit/s), with the known frame rate (fps), the number of video frames T , and the temporal stride Δt , by $\tilde{b} = \frac{8 \sum_{i=1}^T \tilde{f}_i \text{ fps}}{T \Delta t}$, assuming a constant stream for the duration of the input clip. We use a small ϵ_B in order to enforce the generated bandwidth to be just below the available bandwidth.

The performance loss enforces the preservation of downstream vision performance. In the case of optical flow estimation, we use a scaled absolute error loss $H(b - \tilde{b}(1 + \epsilon_p)) \|\mathbf{O} - \tilde{\mathbf{O}}\|_1$. \mathbf{O} denotes the optical flow prediction for the coded video clip and $\tilde{\mathbf{O}}$ represents the optical flow prediction based on the original (raw) video clip, used as a pseudo label. We scale the absolute error with a Heaviside function H , only considering the server-side model’s performance if the target bandwidth is met with a small tolerance ϵ_p . For semantic segmentation, we replace the absolute error with the Kullback–Leibler divergence. Note that using a different server-side model (e.g. object detection model) can require adapting \mathcal{L}_p to the new task.

During preliminary experiments, we observed the control network can struggle to use the whole range of QP values. Motivated by this observation, we regularize the control network toward generating a bitrate close to the target by

$$\mathcal{L}_r = |\min(0, \tilde{b} - b(1 - \epsilon_r))|. \quad (8)$$

This regularization loss penalizes the control network if the bandwidth prediction \tilde{b} is far away from the target bandwidth b . We utilize $\epsilon_B < \epsilon_r$ to not push the generated bandwidth above the target bandwidth.

Training schedule We train both our deep codec control and surrogate in an alternating fashion. To ensure a stable training of our control network from the beginning on, we pre-train the surrogate model before fine-tuning it during the control training. The codec control training is depicted in pseudocode in the supplement. Note, that our H.264 surrogate is only required for training, not for inference. For inference, the standard H.264 codec is used. We maintain an exponential moving average of the control network (w/ a decay of 0.99) to combat the noise in our learning signal introduced by our surrogate and the Gumbel-Softmax trick.

Discussion. We propose to learn high-dimensional codec parameters using end-to-end self-supervised learning, directly optimizing our control objective (Equation (1)). However, learning codec parameters could theoretically also be achieved using reinforcement learning (RL) (Mandhane et al., 2022). We argue that using RL is infeasible due to the high-dimensional action space (codec parameters) and the complex loss surface of downstream vision model (Buşoniu et al., 2018; Li et al., 2018). Note that our deep codec control training can be also viewed as a kind of knowledge distillation (Gao et al., 2021). We learn our control network with knowledge distilled from the downstream model.

4. Experiments

Dataset. We perform experiments on Cityscapes (Cordts et al., 2016) and CamVid (Brostow et al., 2009). We utilize

the unlabeled sequences of Cityscapes including 30-frame video clips ($\sim 10k$ frames total) with 2967 training and 498 validation clips. The frame rate is 17fps. Similarly for Camvid, we use the available videos (at 15fps) composed of $\sim 29k$ frames in total. We use three videos for training and one video for validation. For codec control training & validation, we sample clips of 8 frames with a temporal stride of 3. For the surrogate model pre-training, we vary the temporal stride randomly between 1, 2, and 3.

Baseline. Since we are not aware of an existing general or task-specific approach to directly solve our constrained optimization problem (*cf.* Equation (1)) within the scope of standardization, we utilize the generic H.264 rate control. In particular, we follow similar work and use 2-pass average bitrate (ABR) rate control (Tomar, 2006; Mandhane et al., 2022). 2-pass ABR is a competitive baseline, since, in contrast to our control, 2-pass ABR consumes the video clip twice. The first pass gathers information about the motion and prediction error. The second pass uses this information to set QP for meeting the target bandwidth while minimizing distortion. Note that 2-pass ABR does not guarantee that the target bandwidth is met.

Control validation. We aim to validate the codec controls directly on the constrained optimization problem (*cf.* Equation (1)) by measuring a task-specific metric, considering clip dropping. In a real-world deployment, exceeding the available network bandwidth can result in block noises, frame skipping, or even clip dropping (worst case) (Itsumi et al., 2022). For validating segmentation performance we use the pixel-wise accuracy acc_{seg} (in %) considering clip-dropping if bandwidth is exceeded. If a clip is dropped acc_{seg} is considered to be zero for the respective clip. For optical flow estimation, we use the F1-all metric, reporting the outlier ratio (in %) of pixels exceeding a threshold of 3 pixels or 5% w.r.t. the optical flow (pseudo) label. If bandwidth is exceeded we set F1-all to 100% for the respective clip. Note we employ the prediction on the original (uncomp.) clip as a pseudo label. In addition to the task-specific metric, we also measure the bandwidth condition accuracy acc_{bw} (in %). Following similar work, we measure both the task-specific metric (acc_{seg} or F1-all) and acc_{bw} with a tolerance of zero ($\Delta 0\%$), five ($\Delta 2\%$), and ten ($\Delta 5\%$) percent on the bandwidth condition (Mandhane et al., 2022).

Implementation details. We implement our surrogate model and codec control pipeline using PyTorch (Paszke et al., 2019) and PyTorch Lightning (Falcon & The PyTorch Lightning Team, 2019). For the macroblock-wise H.264 compression, we rely on the modified FFMpeg implementation of AccMPEG (Tomar, 2006; Du et al., 2022). We pre-train our surrogate model for 45k iterations. Our deep codec control is trained for just 6.0k iterations. For both,



Figure 6. Qualitative surrogate model results. On the left frame coded by H.264 for the given QP map (right). In the middle is the coded video prediction of our surrogate model. We show the first frame of the clip. CamVid dataset used.

we utilize two NVIDIA A6000 (48GB) GPUs. Surrogate pre-training takes approximately one day, whereas the codec control training requires 16h to complete. We sample the network bandwidth condition b from a log uniform distribution \mathcal{U}_{\log} (30kbit/s, 0.9Mbit/s) capturing the working range of the H.264 codec. We sample from a log-uniform distribution to explore QP uniformly during training. For more implementation details and hyperparameters please refer to the supplement.

Surrogate model results. In Figure 6, we showcase qualitative results of our codec surrogate model in approximating H.264 video distortion. Our conditional surrogate can adapt to different macroblock-wise quantization parameters and accurately approximate video distortion introduced by H.264. For low QP regions, our conditional surrogate maintains details of the video frame. For high QP regions, details and high-frequencies are discarded and the video is distorted similarly to the original coded video.

We also validate the effectiveness of our conditional H.264 surrogate model qualitatively (*cf.* Table 2). In addition, we also ablate the effect of our AGRU bottleneck block. For comparison, we train a conditional surrogate model with three standard 3D residual blocks, instead of our AGRU, in the bottleneck stage. Our conditional surrogate model

Table 2. Conditional surrogate model validation results. We report SSIM and L1 scores for the distorted video prediction and the relative error for the file size prediction. Note a pixel range of $[0, 255]$ is used for validation. We show results averaged over the full QP range. We validate the surrogate model once on each possible QP value using a uniform QP (for all macroblocks).

Method	AGRU	\tilde{V}		\tilde{f}
		SSIM \uparrow	L1 \downarrow	Rel. error (%) \downarrow
<i>Cityscapes</i> (Cordts et al., 2016)				
Conditional surrogate	✗	0.949	3.892	6.719
Conditional surrogate	✓	0.964	2.552	5.150
<i>CamVid</i> (Brostow et al., 2009)				
Conditional surrogate	✓	0.958	2.876	2.246

Table 3. Semantic segmentation validation results. BW (acc_{bw}) & segmentation accuracies (acc_{seg}) for difference BW tolerances reported. Metrics averaged over ten different BW conditions.

Method	acc_{bw} (%) \uparrow			acc_{seg} (%) \uparrow		
	$\Delta 0\%$	$\Delta 2\%$	$\Delta 5\%$	$\Delta 0\%$	$\Delta 2\%$	$\Delta 5\%$
<i>Cityscapes</i> (Cordts et al., 2016)						
2-pass ABR (H.264)	68.13	74.98	82.31	64.29	70.57	77.07
Deep codec control	96.22	97.05	97.91	84.79	85.50	86.28
<i>CamVid</i> (Brostow et al., 2009)						
2-pass ABR (H.264)	63.91	74.43	85.36	54.06	62.49	71.53
Deep codec control	94.64	95.61	96.46	65.70	62.52	59.01

is able to approximate the codec video of standard H.264 well. Additionally, our conditional surrogate model also accurately predicts the generated file size. Using our AGRU improves over the 3D convolutional baseline. Note we offer additional results of our surrogate in the supplement.

Codec control results: semantic segmentation. We compare our deep codec control to 2-pass ABR on the downstream task of semantic segmentation. As the downstream model, we utilize a DeepLabV3 model (w/ ResNet-18 backbone) trained on the respective dataset. Our obtained results are depicted in Table 3. On both the Cityscapes and CamVid dataset our deep codec control strongly outperforms the 2-pass ABR control. Our deep codec control better preserves downstream performance (with no bandwidth tolerance) and predicts codec parameters such that the dynamic bandwidth condition is met. In contrast, 2-pass ABR tends to overshoot the bandwidth condition. This can be observed by the vastly increasing acc_{bw} if a bandwidth tolerance is permitted. This behavior is also reflected in an increased segmentation accuracy (considering drops) of 2-pass ABR if a bandwidth tolerance is permitted. However, in the most representative case, if no bandwidth tolerance is permitted, our deep codec control leads to vastly better downstream results. In particular, on Cityscapes our deep codec control leads to improvements in acc_{seg} of 18.6% and on CamVid to 11.6% over 2-pass ABR considering no BW tolerance.

Codec control results: optical flow estimation. We also analyze the performance of deep codec control and our 2-pass ABR baseline on optical flow estimation as the downstream vision task. As the downstream model, we utilize RAFT (large), trained on synthetic data and driving data of the KITTI dataset (Geiger et al., 2013; Teed & Deng, 2020). Table 4 presents our codec control results for optical flow estimation. Similar to semantic segmentation, our codec control also outperforms 2-pass ABR in controlling H.264 for optical flow estimation. Our deep codec control better preserves downstream performance (w/ no bandwidth tolerance) and better follows dynamic bandwidth conditions.

Table 4. Optical flow validation results. We report bandwidth accuracy (acc_{bw}) and F1-all scores for difference tolerances on the BW conditions. Metrics averaged over different ten BW conditions.

Method	acc_{bw} (%) \uparrow			F1-all (%) \downarrow		
	$\Delta 0\%$	$\Delta 2\%$	$\Delta 5\%$	$\Delta 0\%$	$\Delta 2\%$	$\Delta 5\%$
<i>Cityscapes</i> (Cordts et al., 2016)						
2-pass ABR (H.264)	69.60	76.48	83.09	41.99	36.37	31.18
Deep codec control	98.05	98.29	98.86	27.57	27.42	27.03
<i>CamVid</i> (Brostow et al., 2009)						
2-pass ABR (H.264)	63.99	73.93	85.34	43.54	34.73	26.31
Deep codec control	97.41	98.73	98.09	21.06	20.55	20.08

Table 5. Transfer results of our codec control from optical flow estimation to semantic segmentation on Cityscapes. For reference, we also report results when directly trained on semantic segmentation.

Training task	acc_{bw} \uparrow			acc_{seg} \uparrow		
	$\Delta 0\%$	$\Delta 2\%$	$\Delta 5\%$	$\Delta 0\%$	$\Delta 2\%$	$\Delta 5\%$
Optical flow estimation	97.79	98.31	98.90	75.03	75.37	75.76
Semantic segmentation	96.22	97.05	97.91	84.79	85.50	86.28

Since the 2-pass ABR control often overshoots the bandwidth condition downstream performance is increased if a bandwidth tolerance is permitted. If no bandwidth tolerance is permitted, the most representative setting, our deep codec control leads to more than 10% fewer outliers (F1-all) in the optical flow prediction than 2-pass ABR.

Codec control transfer results In Table 5, we report results when transferring our deep codec control between downstream tasks during inference. When transferring our deep codec control trained to preserve optical flow performance to semantic segmentation we observe a drop in performance. This demonstrates both the ability of our codec control to learn a task-specific behavior and showcases the effectiveness of the surrogate model’s gradients.

Additional results. We refer the reader to the supplement for additional (qualitative & quantitative) results of both our deep video codec control and conditional surrogate model.

5. Related Work

Video compression. The inherent memory complexity and temporal redundancy of video data have motivated the development of numerous algorithms for compressing videos (Wu et al., 2001; Richardson, 2011; Liu et al., 2020). Significant time has been dedicated to the development of standardized video compression algorithms, examples include H.264 (Wiegand et al., 2003), H.265 (Sullivan et al., 2012), and MPEG-5 (Choi et al., 2020). Recently, deep learning-based video compression algorithms have been in-

roduced (Wood, 2022; Zhang et al., 2023). Despite offering better preservation of the perceptual quality in the coded video and supporting custom quality objectives (*e.g.*, preserving downstream performance), deep video compression algorithms find minimal applicability, as they lack widely supported standardization, are computationally heavy, and offer limited customizability as well as control over the compression process for rate control (Zhang et al., 2023).

Video compression for machines. With an increasing amount of video data being analyzed by machines, such as deep vision models, a new line of research on video compression for machines has emerged (Duan et al., 2020). A common approach is to extract vision feature maps from an image or video and perform compression at the feature level (Emmons et al., 2019; Matsubara et al., 2019; Duan et al., 2020; Xia et al., 2020). Another approach is to train a deep compression algorithm for a specific vision task, such as object detection (Beye et al., 2022). While some efforts have been made towards standardizing video compression for machines, no general standard has emerged yet (Duan et al., 2020; Gao et al., 2021; Wood, 2022), and the applicability of such approaches remains very limited. We do not aim to develop a new video codec for machines, rather our aim is to control widely used standard codecs for deep vision models as content and network bandwidth changes.

Video codec control for vision models. A common approach for identifying regions of interest for vision tasks is to utilize local and simple heuristics (Zhang et al., 2018; Li et al., 2020). Hard-coded rules are used to decide how to set the codec control (Zhang et al., 2018; Li et al., 2020). These approaches implicitly assume static scenes and trivially fail on dynamic scenes. Other more sophisticated approaches utilize feedback from a server-side vision model during inference for controlling the encoding (Liu et al., 2019; Du et al., 2020; Zhang et al., 2021). Feedback loop-based approaches entail complicated architectures, add additional points of failure, can break standardization, and often only support a specific vision task. Mandhane et al. (2022) use the MuZero reinforcement learning algorithm to learn a codec control. This control predicts a single codec parameter for each frame under a bandwidth constraint and aims to optimize perceptual quality but does not target vision models. Itsumi et al. (2022) propose an RL approach for finding regions relevant to a vision model. Paired with hard-coded rules they presented a codec control for H.265. While they consider relevant regions for a deep vision model Itsumi et al. do not consider a dynamic bandwidth constraint. AccMPEG (Du et al., 2022) and Galteri et al. (2018) also estimate regions relevant for a deep vision model by learning to predict saliency maps (Simonyan et al., 2013). These approaches also do not consider a bandwidth condition, use hard-coded rules for the control, and are limited by the

concept of saliency maps (Sundararajan et al., 2017).

Video codec surrogate. Standard video codecs, such as H.264 and H.265, are not differentiable w.r.t. the input video and codec parameters. This non-differentiability has motivated the use of deep neural networks to approximate standard codecs in a differentiable manner (Zhao et al., 2019; Qiu et al., 2021; Klopp et al., 2021; Tian et al., 2021; Isik et al., 2023). For instance, Tian et al. (2021) proposed a differentiable surrogate of H.265 that predicts the coded video, for a small subset of clip-wise compression strengths. While we are not the first to learn a differentiable approximation of a standard video codec, we present the first conditional surrogate with support for fine-grain macroblock-wise quantization and offer a differentiable file size prediction.

6. Discussion

We demonstrated the general feasibility of our deep codec control in overcoming the limitations of the standard H.264 codec and conserving downstream performance. Our experiments demonstrate compelling results for two classical downstream tasks: semantic segmentation and optical flow estimation. However, currently, we train a deep codec control for a specific downstream task and model. Training a deep control for every task and model might not be practical. An avenue for future investigation lies in exploring how control networks can be transferred across different downstream tasks and models. Showcasing the potential application to control other video codecs, such as H.265, also represents an interesting direction for future research. Our deep codec control pipeline offers a solid foundation for future research toward cross-task support, a generalized deep codec control, and support for other standard video codecs. We hope that our contribution opens up new avenues in video coding and enables the effective use of standard codecs in state-of-the-art computer vision pipelines.

7. Conclusion

We presented the first fully end-to-end learnable deep codec control for standard video codecs, to conserve downstream deep vision performance in the face of dynamic bandwidth conditions. Our novel conditional differentiable codec surrogate model enables us to learn a content and network bandwidth-dependent codec control using self-supervised learning. We empirically demonstrate that our deep codec control can control the standard H.264 codec and is able to meet dynamic bandwidth conditions, while better preserving the downstream performance of a deep vision model than a standard baseline (H.264 2-pass ABR control). Our deep video codec control not only offers an alternative approach for optimizing video codecs for deep vision models but we can also conserve current standards.

8. Broader Impact

Our deep video codec control offers a novel approach for optimizing standard video codecs for downstream deep vision models, with the potential to improve the latter’s performance. However, we would like to acknowledge the potential ramifications of our approach in real-world settings and highlight two aspects of this. Considering that our deep video codec control training can be interpreted as a form of knowledge distillation (Gou et al., 2021), it is possible for our control network to inherit biases from the downstream model. Therefore, when deployed in real-world applications, a thorough validation process for the control network is essential to prevent biased predictions.

Despite the potential risks, deploying our deep video codec control has the capability to enhance the analysis of coded video. Specifically, safety-critical applications, such as autonomous driving, could experience substantial benefits from our improved video analytics.

References

- Araslanov, N. and Roth, S. Self-supervised Augmentation Consistency for Adapting Semantic Segmentation. In *CVPR*, pp. 15384–15394, 2021.
- Ballas, N., Yao, L., Pal, C., and Courville, A. C. Delving deeper into convolutional networks for learning video representations. In *ICLR*, 2016.
- Barnett, T., Jain, S., Andra, U., and Khurana, T. Cisco Visual Networking Index (VNI) Complete Forecast Update. *Americas/EMEAR CKN Presentation*, pp. 1–30, 2018.
- Beye, F., Itsumi, H., Vitthal, C., and Nihei, K. Recognition-Aware Deep Video Compression for Remote Surveillance. In *ICIP*, pp. 1986–1990, 2022.
- Brostow, G. J., Fauqueur, J., and Cipolla, R. Semantic object classes in video: A high-definition ground truth database. *Pattern Recognit. Lett.*, 30(2):88–97, 2009.
- Buřoniu, L., de Bruin, T., Tolić, D., Kober, J., and Palunko, I. Reinforcement Learning for Control: Performance, Stability, and Deep Approximators. *Annu. Rev. Control.*, 46:8–28, 2018.
- Chen, L.-C., Papandreou, G., Schroff, F., and Adam, H. Rethinking Atrous Convolution for Semantic Image Segmentation. *arXiv preprint arXiv:1706.05587*, 2017.
- Choi, K., Chen, J., Rusanovskyy, D., Choi, K.-P., and Jang, E. S. An Overview of the MPEG-5 Essential Video Coding Standard. *IEEE Signal Process. Mag.*, 37(3):160–167, 2020.
- Cordts, M., Omran, M., Ramos, S., Rehfeld, T., Enzweiler, M., Benenson, R., Franke, U., Roth, S., and Schiele, B. The Cityscapes Dataset for Semantic Urban Scene Understanding. In *CVPR*, pp. 3213–3223, 2016.
- de Vries, H., Strub, F., Mary, J., Larochelle, H., Pietquin, O., and Courville, A. C. Modulating early visual processing by language. In *NIPS*, volume 30, 2017.
- Du, K., Pervaiz, A., Yuan, X., Chowdhery, A., Zhang, Q., Hoffmann, H., and Jiang, J. Server-Driven Video Streaming for Deep Learning Inference. In *SIGCOMM*, pp. 557–570, 2020.
- Du, K., Zhang, Q., Arapin, A., Wang, H., Xia, Z., and Jiang, J. AccMPEG: Optimizing Video Encoding for Accurate Video Analytics. In *MLSys*, volume 4, pp. 450–466, 2022.
- Duan, L., Liu, J., Yang, W., Huang, T., and Gao, W. Video Coding for Machines: A Paradigm of Collaborative Compression and Intelligent Analytics. *IEEE Trans. Image Process.*, 29:8680–8695, 2020.
- Emmons, J., Fouladi, S., Ananthanarayanan, G., Venkataraman, S., Savarese, S., and Winstein, K. Cracking open the DNN black-box: Video Analytics with DNNs across the Camera-Cloud Boundary. In *MobiCom HotEdgeVideo Workshop*, pp. 27–32, 2019.
- Falcon, W. and The PyTorch Lightning Team. PyTorch Lightning. <https://github.com/Lightning-AI/lightning>, 2019.
- Fan, H., Murrell, T., Wang, H., Alwala, K. V., Li, Y., Li, Y., Xiong, B., Ravi, N., Li, M., Yang, H., et al. PyTorchVideo: A Deep Learning Library for Video Understanding. In *ACMMM*, pp. 3783–3786, 2021.
- Feichtenhofer, C. X3D: Expanding Architectures for Efficient Video Recognition. In *CVPR*, pp. 203–213, 2020.
- Galteri, L., Bertini, M., Seidenari, L., and Del Bimbo, A. Video Compression for Object Detection Algorithms. In *ICPR*, pp. 3007–3012, 2018.
- Gao, W., Liu, S., Xu, X., Rafie, M., Zhang, Y., and Curcio, I. Recent Standard Development Activities on Video Coding for Machines. *arXiv preprint arXiv:2105.12653*, 2021.
- Geiger, A., Lenz, P., Stiller, C., and Urtasun, R. Vision meets Robotics: The KITTI Dataset. *Int. J. Robot. Res.*, 32(11):1231–1237, 2013.
- Glynn, P. W. and Szechtman, R. Some New Perspectives on the Method of Control Variates. In *Monte Carlo and Quasi-Monte Carlo Methods 2000*, pp. 27–49. Springer, 2002.

- Gou, J., Yu, B., Maybank, S. J., and Tao, D. Knowledge Distillation: A Survey. *IJCV*, 129:1789–1819, 2021.
- Grathwohl, W., Choi, D., Wu, Y., Roeder, G., and Duvenaud, D. Backpropagation through the Void: Optimizing control variates for black-box gradient estimation. In *ICLR*, 2018.
- He, K., Zhang, X., Ren, S., and Sun, J. Deep Residual Learning for Image Recognition. In *CVPR*, pp. 770–778, 2016.
- Hu, M., Luo, Z., Pasdar, A., Lee, Y. C., Zhou, Y., and Wu, D. Edge-Based Video Analytics: A Survey. *arXiv preprint arXiv:2303.14329*, 2023.
- Isik, B., Guleryuz, O. G., Tang, D., Taylor, J., and Chou, P. A. Sandwiched Video Compression: Efficiently Extending the Reach of Standard Codecs with Neural Wrappers. *arXiv preprint arXiv:2303.11473*, 2023.
- Isumi, H., Beye, F., Charvi, V., and Nihei, K. Learning Important Regions via Attention for Video Streaming on Cloud Robotics. In *IROS*, 2022.
- Jang, E., Gu, S., and Poole, B. Categorical Reparameterization with Gumbel-Softmax. In *ICLR*, 2017.
- Jeong, J., Cai, H., Garrepalli, R., and Porikli, F. Distract-Flow: Improving Optical Flow Estimation via Realistic Distractions and Pseudo-Labeling. In *CVPR*, pp. 13691–13700, 2023.
- Jiang, L., Dai, B., Wu, W., and Loy, C. C. Focal Frequency Loss for Image Reconstruction and Synthesis. In *ICCV*, pp. 13919–13929, 2021.
- Klopp, J. P., Liu, K.-C., Chen, L.-G., and Chien, S.-Y. How to Exploit the Transferability of Learned Image Compression to Conventional Codecs. In *CVPR*, pp. 16165–16174, 2021.
- Lampert, C. H. Machine Learning for Video Compression: Macroblock Mode Decision. In *ICPR*, volume 1, pp. 936–940, 2006.
- Lederer, S. 2019 Video Developer Report – The Future of Video: AV1 Codec, AI & Machine Learning, and Low Latency. <https://bitmovin.com/bitmovin-2019-video-developer-report-av1-codec-ai-machine-learning-low-latency/>, 2019.
- Li, H., Xu, Z., Taylor, G., Studer, C., and Goldstein, T. Visualizing the Loss Landscape of Neural Nets. In *NeurIPS*, volume 31, 2018.
- Li, Y., Padmanabhan, A., Zhao, P., Wang, Y., Xu, G. H., and Netravali, R. Reducto: On-Camera Filtering for Resource-Efficient Real-Time Video Analytics. In *SIGCOMM*, pp. 359–376, 2020.
- Liu, D., Li, Y., Lin, J., Li, H., and Wu, F. Deep Learning-Based Video Coding: A Review and a Case Study. *ACM Comput. Surv.*, 53(1):1–35, 2020.
- Liu, L., Li, H., and Gruteser, M. Edge Assisted Real-time Object Detection for Mobile Augmented Reality. In *ACM MobiCom*, pp. 1–16, 2019.
- Loshchilov, I. and Hutter, F. SGDR: Stochastic Gradient Descent with Warm Restarts. In *ICLR*, 2017.
- Luo, X., Talebi, H., Yang, F., Elad, M., and Milanfar, P. The Rate-Distortion-Accuracy Tradeoff: JPEG Case Study. In *DCC*, pp. 354–354, 2021.
- Maas, A. L., Hannun, A. Y., Ng, A. Y., et al. Empirical Evaluation of Rectified Activations in Convolutional Network. In *ICML*, volume 30, pp. 3, 2013.
- Mandhane, A., Zhernov, A., Rauh, M., Gu, C., Wang, M., Xue, F., Shang, W., Pang, D., Claus, R., Chiang, C.-H., et al. MuZero with Self-competition for Rate Control in VP9 Video Compression. *arXiv preprint arXiv:2202.06626*, 2022.
- Matsubara, Y., Baidya, S., Callegaro, D., Levorato, M., and Singh, S. Distilled Split Deep Neural Networks for Edge-Assisted Real-Time Systems. In *MobiCom HotEdgeVideo Workshop*, pp. 21–26, 2019.
- MMSegmentation Contributors. MMSegmentation: Open-MMLab Semantic Segmentation Toolbox and Benchmark. <https://github.com/open-mmlab/mms Segmentation>, 2020.
- Nah, S., Baik, S., Hong, S., Moon, G., Son, S., Timofte, R., and Mu Lee, K. NTIRE 2019 Challenge on Video Deblurring and Super-Resolution: Dataset and Study. In *CVPRW*, 2019.
- Nair, V. and Hinton, G. E. Rectified Linear Units Improve Restricted Boltzmann Machines. In *ICML*, pp. 807–814, 2010.
- Otani, A., Hashiguchi, R., Omi, K., Fukushima, N., and Tamaki, T. Performance Evaluation of Action Recognition Models on Low Quality Videos. *IEEE Access*, 10: 94898–94907, 2022.
- Paszke, A., Gross, S., Massa, F., Lerer, A., Bradbury, J., Chanan, G., Killeen, T., Lin, Z., Gimelshein, N., Antiga, L., et al. PyTorch: An Imperative Style, High-Performance Deep Learning Library. *NeurIPS*, 32, 2019.
- Qiu, K., Yu, L., and Li, D. Codec-Simulation Network for Joint Optimization of Video Coding With Pre- and Post-Processing. *IEEE Open J. Circuits Syst.*, 2:648–659, 2021.

- Riba, E., Mishkin, D., Ponsa, D., Rublee, E., and Bradski, G. Kornia: an Open Source Differentiable Computer Vision Library for PyTorch. In *WACV*, pp. 3674–3683, 2020.
- Richardson, I. E. *H.264 and MPEG-4 Video Compression: Video Coding for Next-generation Multimedia*. John Wiley & Sons, 2004.
- Richardson, I. E. *The H. 264 Advanced Video Compression Standard*. John Wiley & Sons, 2011.
- Ronneberger, O., Fischer, P., and Brox, T. U-Net: Convolutional Networks for Biomedical Image Segmentation. In *MICCAI*, pp. 234–241, 2015.
- Simonyan, K., Vedaldi, A., and Zisserman, A. Deep Inside Convolutional Networks: Visualising Image Classification Models and Saliency Maps. *arXiv preprint arXiv:1312.6034*, 2013.
- Sullivan, G. J., Ohm, J.-R., Han, W.-J., and Wiegand, T. Overview of the High Efficiency Video Coding (HEVC) Standard. *IEEE Trans. Circuits Syst. Video Technol.*, 22(12):1649–1668, 2012.
- Sundararajan, M., Taly, A., and Yan, Q. Axiomatic Attribution for Deep Networks. In *ICML*, pp. 3319–3328, 2017.
- Teed, Z. and Deng, J. RAFT: Recurrent All-Pairs Field Transforms for Optical Flow. In *ECCV*, pp. 402–419, 2020.
- Tian, Y., Lu, G., Min, X., Che, Z., Zhai, G., Guo, G., and Gao, Z. Self-Conditioned Probabilistic Learning of Video Rescaling. In *ICCV*, pp. 4490–4499, 2021.
- Tomar, S. Converting Video Formats with FFmpeg. *Linux J.*, 2006(146):10, 2006.
- TorchVision Maintainers and Contributors. TorchVision: PyTorch’s Computer Vision library. <https://github.com/pytorch/vision>, 2016.
- Vaswani, A., Shazeer, N., Parmar, N., Uszkoreit, J., Jones, L., Gomez, A. N., Kaiser, L. u., and Polosukhin, I. Attention is All you Need. In *NIPS*, volume 30, 2017.
- Wallace, G. K. The JPEG still picture compression standard. *IEEE Trans. Consum. Electron.*, 38(1):xviii–xxxiv, 1992.
- Wang, X., Yu, K., Dong, C., and Loy, C. C. Recovering Realistic Texture in Image Super-resolution by Deep Spatial Feature Transform. In *CVPR*, pp. 606–615, 2018.
- Wang, Z., Bovik, A. C., Sheikh, H. R., and Simoncelli, E. P. IEEE Transactions on Image Processing. *IEEE Trans. Image Process.*, 13(4):600–612, 2004.
- Wiegand, T., Sullivan, G. J., Bjontegaard, G., and Luthra, A. Overview of the H.264/AVC Video Coding Standard. *IEEE Trans. Circuits Syst. Video Technol.*, 13(7):560–576, 2003.
- Wood, D. Task Oriented Video Coding: A Survey. *arXiv preprint arXiv:2208.07313*, 2022.
- Wu, D., Hou, Y. T., Zhu, W., Zhang, Y.-Q., and Peha, J. M. Streaming Video over the Internet: Approaches and Directions. *IEEE Trans. Circuits Syst. Video Technol.*, 11(3):282–300, 2001.
- Wu, Y. and He, K. Group Normalization. In *ECCV*, pp. 3–19, 2018.
- Xia, S., Liang, K., Yang, W., Duan, L.-Y., and Liu, J. An Emerging Coding Paradigm VCM: A Scalable Coding Approach Beyond Feature and Signal. In *ICME*, pp. 1–6, 2020.
- Xie, X., Zhou, N., Zhu, W., and Liu, J. Bandwidth-Aware Adaptive Codec for DNN Inference Offloading in IoT. In *ECCV*, pp. 88–104, 2022.
- Zhang, B., Jin, X., Ratnasamy, S., Wawrzyniek, J., and Lee, E. A. AWStream: Adaptive Wide-Area Streaming Analytics. In *SIGCOMM*, pp. 236–252, 2018.
- Zhang, W., He, Z., Liu, L., Jia, Z., Liu, Y., Gruteser, M., Raychaudhuri, D., and Zhang, Y. Elf: Accelerate High-resolution Mobile Deep Vision with Content-aware Parallel Offloading. In *ACM MobiCom*, pp. 201–214, 2021.
- Zhang, Y., Zhu, L., Jiang, G., Kwong, S., and Kuo, C.-C. J. A Survey on Perceptually Optimized Video Coding. *ACM Comput. Surv.*, 55(12):1–37, 2023.
- Zhao, H., Gallo, O., Frosio, I., and Kautz, J. Loss Functions for Image Restoration With Neural Networks. *IEEE Trans. Comput. Imaging.*, 3(1):47–57, 2016.
- Zhao, L., Bai, H., Wang, A., and Zhao, Y. Learning a Virtual Codec Based on Deep Convolutional Neural Network to Compress Image. *J. Vis. Commun. Image Represent.*, 63: 102589, 2019.

Supplement

In this supplement, we provide additional details of our deep video codec control and conditional surrogate model. In particular, we present additional material on our methodology and also provide additional experimental results.

A. Method

This section provides additional details about our novel self-supervised control training, the surrogate model pre-training, the conditional group normalization layer, and the encoder/decoder residual block used in our conditional surrogate model. Finally, we provide a more detailed discussion of the novelty of our conditional surrogate model supporting the main paper’s related work section.

A.1. Self-supervised deep codec control

Here we provide our self-supervised control training in PyTorch-like pseudo-code (Algorithm 1). Note, we train our codec control and conditional surrogate model in an alternating fashion. We utilize the prediction on the original uncompressed clip as a pseudo label in our deep codec control training (line 14). More advanced pseudo-labeling approaches (*e.g.*, (Araşlanov & Roth, 2021) or (Jeong et al., 2023)) might offer an improved learning signal. However, for the sake of simplicity, we refrain from using advanced pseudo-labeling approaches.

Algorithm 1 Our end-to-end deep codec control training.

```

1  for clip in data_loader:
2      # Sample BW condition
3      bw_c = log_uniform(bw_min, bw_max)
4      # Make one-hot QP prediction
5      qp_oh = control_network(clip, bw_c)
6      # Forward pass surrogate model
7      clip_c, fs = h264_sg(clip, qp_oh)
8      # Convert file size to BW
9      bw = file_size_to_bandwidth(fs)
10     # Make downstream prediction
11     pred = downstream_model(clip_c)
12     # Downstream prediction raw clip
13     with no_grad():
14         label_pseudo = downstream_model(clip)
15     # Compute loss
16     loss = a_b * l_b(bw, bw_c) \
17         + a_r * regularizer_b(bw, bw_c) \
18         + a_p * h(bw_c - bw) * l_p(pred, label_pseudo)
19     # Backward pass
20     loss.backward()
21     # Optimization step
22     optimizer_control_network.step()
23     # Update EMA control network
24     ema(control_network, control_network_ema, decay=0.99)
25     # Next: Surrogate model training step

```

A.2. Surrogate model pre-training

During preliminary surrogate model pre-training runs, we observed that the surrogate model entails a tendency to be biased toward the identity function. In particular, the surrogate model solved the task of predicting the distorted video by predicting the original video. We combat this behavior by first learning on high quantization parameter (QP) values and gradually introducing a larger range of QP during training. We start by just sampling a macroblock-wise QP of 51 before linearly increasing the QP sampling range to the full range between 0 and 51 until half of the pre-training. We observed that first

learning strong compression rates, including strong video distortion, prevents the surrogate from just learning the identity mapping. We believe the strong video distortion at the beginning of the training lets the conditional surrogate model diverge from the shortcut solution (identity mapping).

To artificially enlarge the number of available video clips, we use data augmentation during surrogate pre-training. In particular, we randomly (with a probability of 0.1) convert the RGB frames to grayscale frames. We also utilize temporal augmentations. We randomly reverse the order of frames (with a probability of 0.5) and repeat frames (with a probability of 0.1).

We sample the QP parameters at different resolution stages to mimic regions with uniform QP values. Additionally, with a probability of 0.4, we utilize the same QP map for all frames in the video clip, mimicking uniform QP values in the spatial dimension. QP sample generated by our technique can be seen in Figure 21 (and subsequent Figures).

A.3. Conditional group normalization

To incorporate the one-hot macroblock-wise quantization parameters \mathbf{qp} into our conditional surrogate model, we utilize conditional group normalization (CGN). Before applying CGN, we embed \mathbf{qp} using a two-layer feed-forward neural network to the latent vector \mathbf{z} . Similar to conditional batch normalization (de Vries et al., 2017), we predict the affine parameters of group normalization (Wu & He, 2018) based on the condition latent vector \mathbf{z} . In particular, we use the spatial feature transform layer introduced by Wang et al. (2018) to predict macroblock-wise affine parameters. Formally, our CGN later is described as

$$\hat{\mathbf{X}} = \text{Softplus}(\xi_\mu(\mathbf{z})) \cdot \text{GroupNorm}(\mathbf{X}) + \xi_\sigma(\mathbf{z}), \quad (9)$$

where \mathbf{X} is the 4D spatio-temporal input feature map and $\hat{\mathbf{X}}$ is the output feature map of the same shape. \mathbf{z} is the 4D condition embedding generated from \mathbf{qp} . ξ denotes a learnable linear mapping transforming the condition embedding. A Softplus activation (Nair & Hinton, 2010) is used to ensure a positive scaling. GroupNorm denotes the standard group normalization layer without affine parameters. To ensure matching spatial dimensions between the feature map and macroblock-wise affine parameters, nearest-neighbor interpolation is used to the output of ξ_μ and ξ_σ .

A.4. Encoder/decoder 2D residual block

Both our surrogate model encoder and decoder utilize 2D residual building blocks (He et al., 2016). In particular, our residual block is composed of two $2\text{D } 3 \times 3$ convolutions, two leaky ReLU activations (Maas et al., 2013), a CGN layer, and a standard GN layer (Wu & He, 2018). In the encoder, we utilize a strided convolution to reduce the spatial dimensions. To upsample the feature maps in the decoder, we employ a 4×4 transposed convolution instead of the first 3×3 convolution. The full block is visualized in Figure 7.

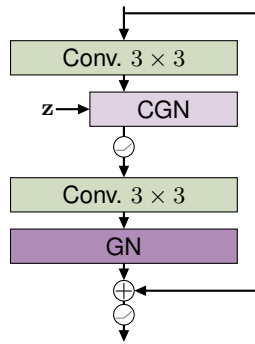


Figure 7. Residual encoder and decoder block conditioned on the latent vector \mathbf{z} .

A.5. Conditional surrogate model discussion.

Note that we are not the first to propose a differentiable surrogate model of a non-differentiable standard video codec (e.g., H.264 or H.265) (Zhao et al., 2019; Qiu et al., 2021; Klopp et al., 2021; Tian et al., 2021; Isik et al., 2023). However, to the best of our knowledge, we are proposing the first surrogate model offering support for fine-grain conditioning (macroblock-wise quantization). Additionally, our conditional surrogate model offers a differentiable prediction of the

file size of the encoded video. While we are the first to offer a differentiable file size prediction for a standard video codec, existing work on surrogate modeling image codecs (*e.g.*, JPEG (Wallace, 1992)) also offers differentiable file size predictions (Luo et al., 2021; Xie et al., 2022). In summary, our novel conditional surrogate model is the first to approximate the H.264 standard video codec while offering macroblock-wise conditioning (over the whole QP range) and a differentiable file size prediction. This conditional surrogate model enables us to learn our deep video codec control in a fully end-to-end fashion, while existing surrogate models are unable to facilitate the end-to-end learning.

B. Experiments

First, we provide additional implementation details, before introducing our downstream models and their downstream performance. Next, we showcase additional results on how H.264 coding affects the downstream performance of deep vision models. Finally, we provide additional deep codec control and surrogate model results.

B.1. Further implementation details

We implement our surrogate model and codec control pipeline using PyTorch (Paszke et al., 2019), PyTorch Lightning (Falcon & The PyTorch Lightning Team, 2019), and Kornia (Riba et al., 2020). For the macroblock-wise H.264 compression, we rely on the modified FFmpeg implementation of AccMPEG (Du et al., 2022; Tomar, 2006). We pre-train our conditional surrogate model for 45k iterations with a base learning rate of $4 \cdot 10^{-4}$ and a weight decay of 10^{-5} . We employ a cosine learning rate schedule with linear annealing (Loshchilov & Hutter, 2017). Our deep codec control is trained for just 4.5k iterations. For training the control network, we also use the AdamW optimizer with a cosine learning rate schedule (without annealing). The base learning rates are set to 10^{-4} for the prediction head and to 10^{-5} for the pre-trained backbone blocks of the control network. We use a weight decay of 10^{-3} . For fine-tuning the conditional surrogate model, we use a fixed learning rate of $1 \cdot 10^{-4}$. For both surrogate pre-training and codec control training, we utilize two NVIDIA A6000 (48GB) GPUs. Surrogate pre-training takes approximately one day, whereas our codec control training requires approximately 12 hours to complete. For both surrogate pre-training and codec control training, we use a batch size of 8 per GPU and half-precision training.

The surrogate model’s encoder uses four residual blocks with 64, 128, 256, and 1024 convolutional filters, respectively. The decoder is composed of four residual blocks with 512, 256, 128, and 64 convolutional filters, respectively. A conditional embedding dimension C_z of 256 is used. The AGRU utilizes a channel dimension of 1024 for each convolution and eight recurrent iterations. For computing the optical flow used to align features before each AGRU iteration, we use a pre-trained RAFT small model from TorchVision (TorchVision Maintainers & Contributors, 2016; Teed & Deng, 2020). We train the RAFT weights together with the other surrogate parameters. For the backbone blocks (X3D-S (Feichtenhofer, 2020)) of the control network (*cf.* Figure 5), we utilize pre-trained weights obtained from action recognition on Kinetics-400 (Fan et al., 2021). We freeze the backbones batch normalization layer during training. For the prediction head, we use two conditional 3D residual blocks (*cf.* Figure 8). During codec control training we start with a Gumbel-Softmax temperature of 2.0 and decrease the temperature in a cosine schedule to 0.1 at the end of the training. In total, the control network is composed of only 3M parameters, making it easier to deploy the control network on an edge device, such as the NVIDIA Jetson Nano.

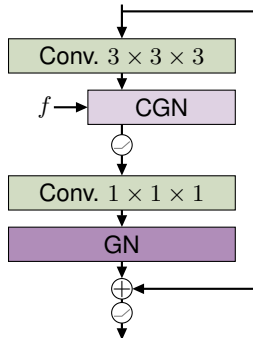


Figure 8. Conditional 3D residual block composed of two convolutions, two leaky ReLU activations, a GN layer, and a CGN layer. For the first convolution, we use a group size equal to the number of channels.

As the segmentation model, we utilize our trained DeepLabV3 models (Cityscapes & CamVid) trained with the MMSeg-

mentation (MMSegmentation Contributors, 2020) protocol and H.264 augmentation. For optical flow estimation, we utilize a RAFT large model from Torchvision (TorchVision Maintainers & Contributors, 2016; Teed & Deng, 2020).

We utilize both Cityscapes (Cordts et al., 2016) and CamVid (Brostow et al., 2009) with a resolution of 224×224 . On Cityscapes, this resolution is achieved by downsampling the frame by a factor of 4 followed by cropping. On CamVid, we downsample the frames by a factor of 3 followed by clipping. We use a resolution of 224×224 to combat the large memory requirements of our codec control pipeline introduced by our surrogate model.

We set the surrogate loss weights to $\alpha_{\rho_v} = 10^{-4}$, $\alpha_{SSIM} = 2$, $\alpha_{FF} = 200$, $\alpha_{\rho_f} = 10^{-4}$, and $\alpha_{L1} = 0.1$. We use $\alpha_p = 2$, $\alpha_b = 6$, $\alpha_r = 1$, $\epsilon_b = \epsilon_p = 0.02$, and $\epsilon_r = 0.05$ for the control loss. We sample the bandwidth condition \tilde{b} from a log uniform distribution $\mathcal{U}_{\log}(30\text{kb}/\text{s}, 0.9\text{Mbit}/\text{s})$ capturing the working range of the H.264 codec (*cf.* Figure 9). We use a log-uniform distribution since the bandwidth correlates logarithmically with QP and we want to explore QP uniformly during training. For validation, we sample 10 bandwidth conditions equally spaced in \log_{10} -space.

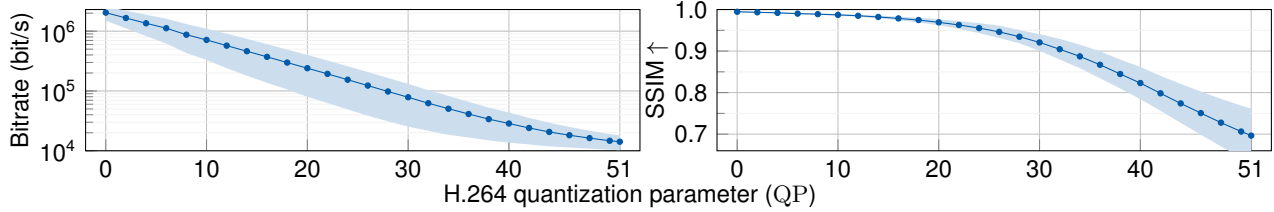


Figure 9. Rate-distortion tradeoff. Bandwidth and SSIM (to raw video) with two standard dev. for different quantization parameters (QP). A uniform QP over all macroblocks is used. Cityscapes (val seq.) with a resolution of 224×224 , a clip length (and GOP) of 8, and a temporal stride of 3 is utilized. Frame rate is 17fps.

B.2. Downstream models

For our semantic segmentation codec control experiments, we utilize a DeepLabV3 (Chen et al., 2017) with ResNet-18 (He et al., 2016) backbone (w/ H.264 aug.). We trained this model on the resolution (224×224) used by our codec control. Additionally, we also trained different variants of the model for analyzing the downstream performance of these models on H.264 codec video. To showcase the effect of H.264 as a data augmentation during downstream training, we train each model variant with and without H.264 as data augmentation. In our H.264 data aug. implementation, we use H.264 coded frames (with random QP) in 50% of the case. Except for the optional addition of the H.264 aug., we follow the Cityscapes training protocol of MMSegmentation (MMSegmentation Contributors, 2020) for both the Cityscapes and the CamVid datasets. Downstream validation results on non-coded frames are shown in Table 6.

Table 6. Downstream model results (semantic segmentation). We report the mean IoU on the respective validation set using the MMSegmentation validation pipeline.

Method	H.264 aug.	mIoU (%) \uparrow
<i>Cityscapes</i> (Cordts et al., 2016)		
DeepLabV3 (ResNet-18)	\times	64.47
DeepLabV3 (ResNet-18)	\checkmark	64.96
DeepLabV3 (ResNet-50)	\times	67.62
DeepLabV3 (ResNet-50)	\checkmark	66.74
<i>CamVid</i> (Brostow et al., 2009)		
DeepLabV3 (ResNet-18)	\times	50.68
DeepLabV3 (ResNet-18)	\checkmark	50.48
DeepLabV3 (ResNet-50)	\times	56.65
DeepLabV3 (ResNet-50)	\checkmark	55.35

For our optical flow codec control experiments, we utilize a RAFT (Teed & Deng, 2020) large model, trained supervised on synthetic data and KITTI (Geiger et al., 2013). In particular, we utilize the public checkpoint from Torchvision (TorchVision Maintainers & Contributors, 2016).

B.3. Deep vision performance on H.264 coded videos

We analyze the performance of our downstream models trained for semantic segmentation on H.264 coded videos. We also analyze the optical flow estimation performance of RAFT (large & small) on coded videos. Cityscapes results are shown in Figure 10. If QP is increased downstream performance on Cityscapes is vastly deteriorated.

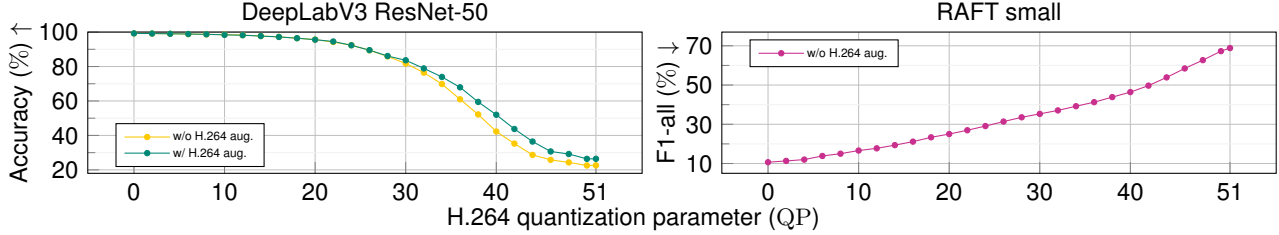


Figure 10. Downstream performance vs. compression trade-off. Cityscapes (val sequences) segmentation accuracy and optical flow estimation performance, measured by average endpoint error (AEPE), for different H.264 quantization parameters between the raw clip predictions (pseudo label) and the compressed clip predictions. Temporal stride is 3 and clip length (and GOP) is 8. QP is applied uniformly.

Downstream performance results on CamVid using H.264 coded videos are shown in Figure 12. Consistent with the results on Cityscapes, downstream performance on CamVid also deteriorates as QP is increased. These findings also align with the findings by Otani et al. (2022) on the deterioration of action recognition performance on H.264 (and JPEG (Wallace, 1992)) coded videos/frames.

Using H.264 coded frames during supervised training only leads to minor residents to coded frames during inference. Still, downstream segmentation performance is highly affected. Interestingly, H.264 augmentation seems to have a better impact if the backbone network has a higher capacity.

B.4. Codec control results: semantic segmentation

We present additional qualitative and quantitative results of our deep video codec control on semantic segmentation as a downstream task. In Figure 11, we showcase our deep codec control on a sequence of 12 video clips of the Cityscapes Stuttgart demo. Our codec control network adapts the macroblock-wise QP to the bandwidth constraints and captures interesting regions. Typically, the control network assigns lower QP values (less compression) to crowded frame regions. Still, the segmentation is affected if only limited bandwidth is available. We also observe the tendency of 2-pass ABR to overshoot the target bandwidth. In contrast, our deep codec control better follows the target bandwidth.

In Figure 13 & Figure 14, we provide fine-grain results to Tab. 1 of the main paper on the Cityscapes dataset. Our deep video codec control largely outperforms 2-pass ABR control. However, for some bandwidth conditions, we perform on par with 2-pass ABR. Surprisingly, we observe that 2-pass ABR not only struggles to meet the bandwidth conditioning for low bandwidth values but also tends to overshoot the target bandwidth for larger bandwidth values.

In Table 7, we ablate the use of EMA on the control networks parameters. While scoring similar bandwidth condition accuracies EMA helps in downstream performance. In the most relevant setting, with no bandwidth tolerance, using EMA improves acc_{seg} by approximately a half percent.

Table 7. EMA ablation results on Cityscapes (semantic segmentation). Here we compare our learn control with and without EMA (exponential moving average) on the parameters. We report bandwidth (acc_{bw}) and segmentation accuracies (acc_{seg}) for difference bandwidth tolerances. Metrics averaged over ten different bandwidth conditions.

Control network EMA	$\text{acc}_{\text{bw}} \uparrow$			$\text{acc}_{\text{seg}} \uparrow$		
	$\Delta 0\%$	$\Delta 5\%$	$\Delta 10\%$	$\Delta 0\%$	$\Delta 5\%$	$\Delta 10\%$
✓	96.22	97.05	97.91	84.79	85.50	86.28
✗	96.12	97.01	96.89	84.36	85.15	86.12

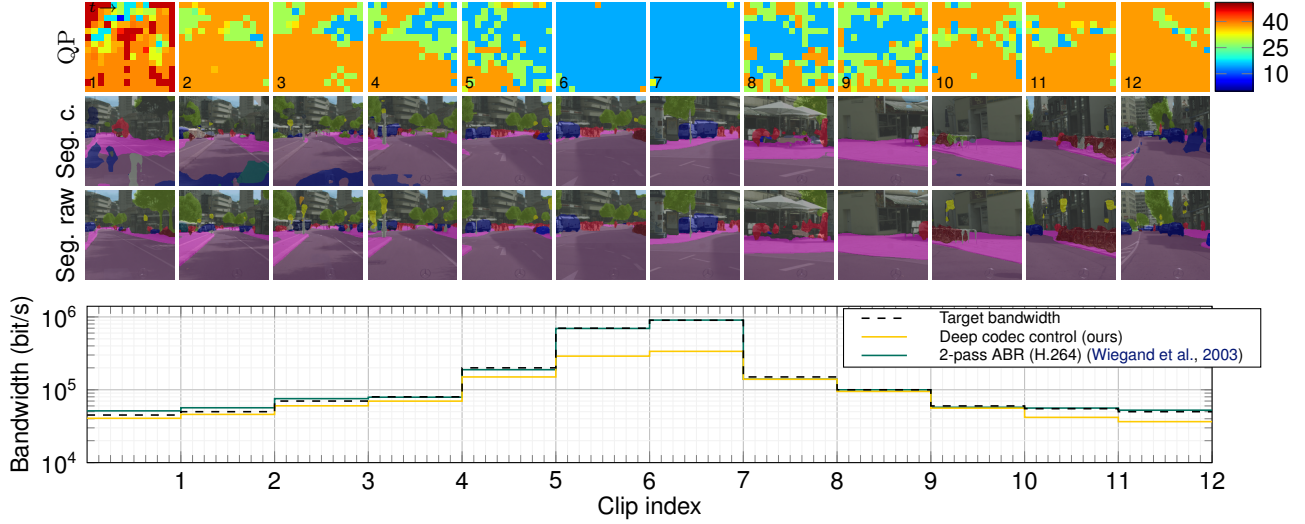


Figure 11. **Qualitative results.** Cityscapes Stuttgart demo (Cordts et al., 2016) with clip-wise varying bandwidth condition. 12 clips with 8 frames each (temp. stride 3) used. QP prediction in the top row, segmentation prediction on the compressed video middle row, and segmentation prediction on the raw video bottom row. For clarity, we only visualize the QP prediction and segmentation for the first frame of each clip. DeepLabV3 (ResNet18 and H.264 aug. training) utilized. The graph shows the generated clip-wise bandwidths by H.264 and our approach. The segmentation accuracy (considering drops) over all clips is 45.71% for H.264 and 82.98% for our deep codec control. Zoom in for details; best viewed in color.

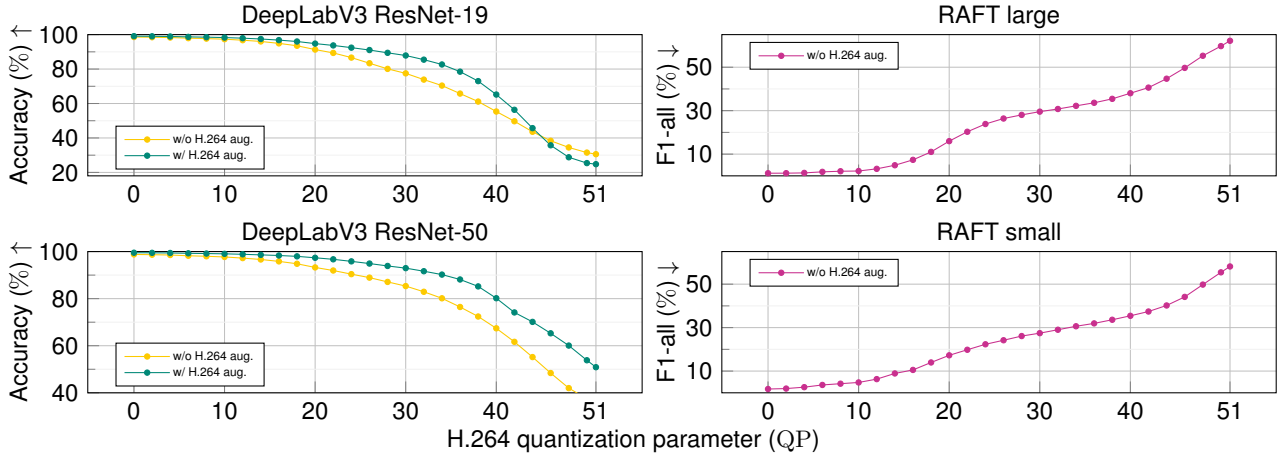


Figure 12. Downstream performance vs. compression trade-off. CamVid (val) segmentation accuracy and optical flow estimation performance, measured by average endpoint error (AEPE), for different H.264 quantization parameters between the raw clip predictions (pseudo label) and the compressed clip predictions. Temporal stride is 3 and clip length (and GOP) is 8. QP is applied uniformly.

B.5. Codec control results: optical flow estimation

In Figure 13 & Figure 14, we provide fine-grain results to Tab. 2 of the main paper on the CamVid dataset. Similar to semantic segmentation, our deep codec control better follows the bandwidth conditioning and also better preserves downstream performance over most of the bandwidth range. Interestingly, for large bandwidth conditions, 2-pass ABR control tends to lead to slightly better downstream results. However, in general, our deep codec control leads to superior results. Especially for low network bandwidth conditions, our deep codec control vastly outperforms 2-pass ABR control.

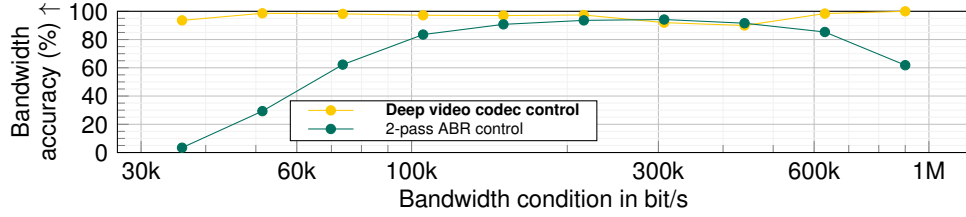


Figure 13. Bandwidth condition results. Bandwidth accuracy (acc_{bw}), i.e., how often the bandwidth constraint has been satisfied, for different network bandwidth conditions on Cityscapes (val sequences).

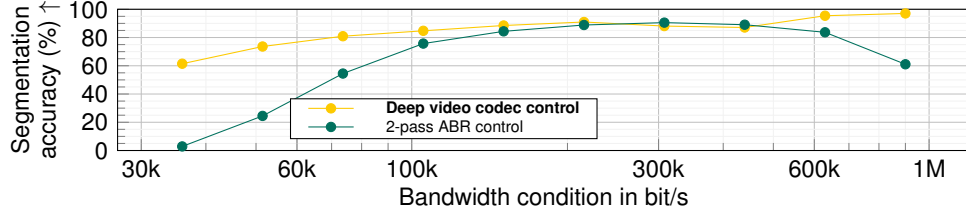


Figure 14. Downstream results. Segmentation accuracy (acc_{seg}), considering clip dropping, for different network bandwidth conditions on Cityscapes (val sequences).

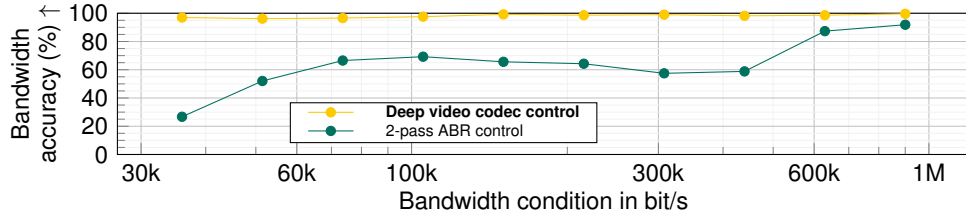


Figure 15. Bandwidth condition results. Bandwidth accuracy (acc_{bw}), i.e., how often the bandwidth constraint has been satisfied, for different network bandwidth conditions on CamVid (val sequences).

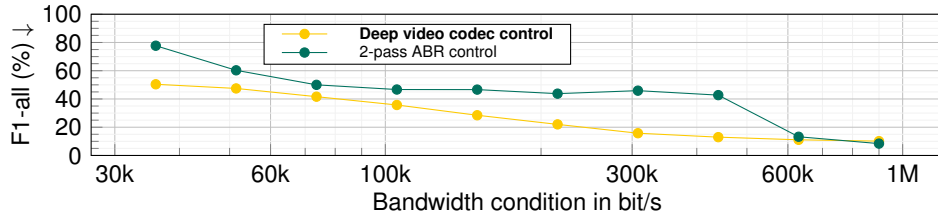


Figure 16. Downstream results. F1-all, considering clip dropping, for different network bandwidth conditions on CamVid (val sequences).

B.6. Surrogate model results

We provide fine-grain results of our conditional surrogate model on CamVid (Figure 17 & Figure 18) and Cityscapes (Figure 19 & Figure 20). Note our conditional surrogate model is considerably better than using the naive solution, the identity function. This can be observed by comparing Figure 17 and Fig. 2 of the main paper.

In the following Figure 21-Figure 26, we provide additional qualitative results of our conditional surrogate in approximating H.264 video distortion for different macroblock-wise quantization parameters. Note we present standard video clips but also show video clips with repeated frames and in reversed order, showcasing the generalization ability of our conditional surrogate model. We observe our surrogate model is able to accurately approximate the video distortion of H.264 for different macroblock-wise quantization parameters.

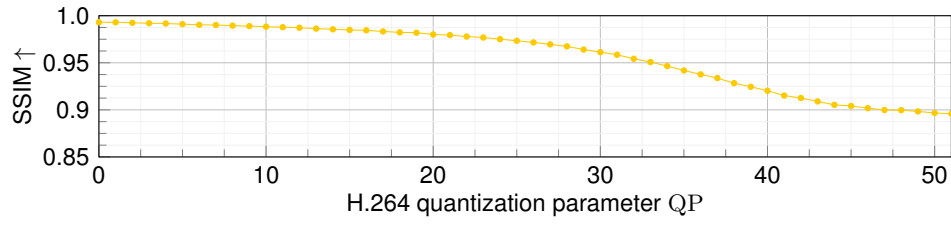


Figure 17. Surrogate model coded video prediction results on CamVid. We utilize a uniform QP (for all macroblocks).

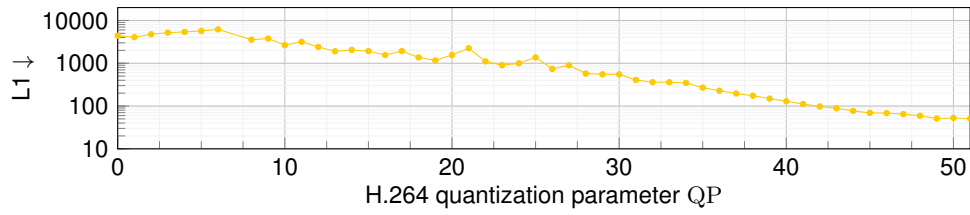


Figure 18. Surrogate model file size prediction results on CamVid. We utilize a uniform QP (for all macroblocks).

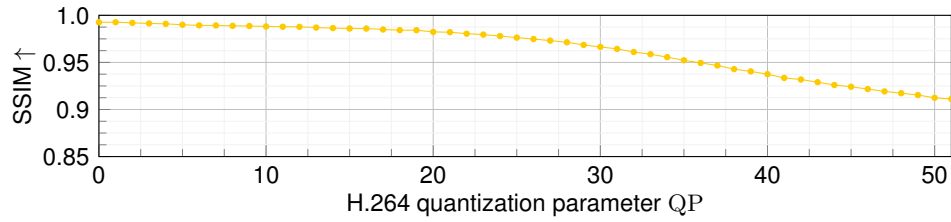


Figure 19. Surrogate model coded video prediction results on CamVid. We utilize a uniform QP (for all macroblocks).

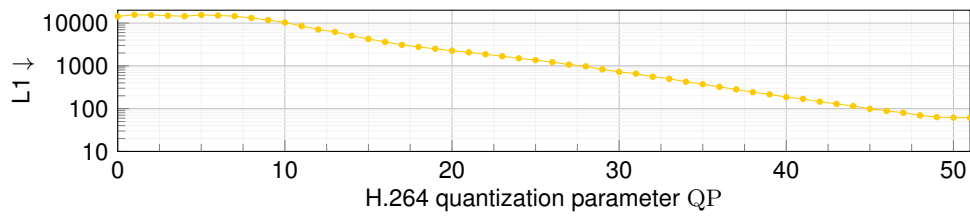


Figure 20. Surrogate model file size prediction results on Cityscapes. We utilize a uniform QP (for all macroblocks).

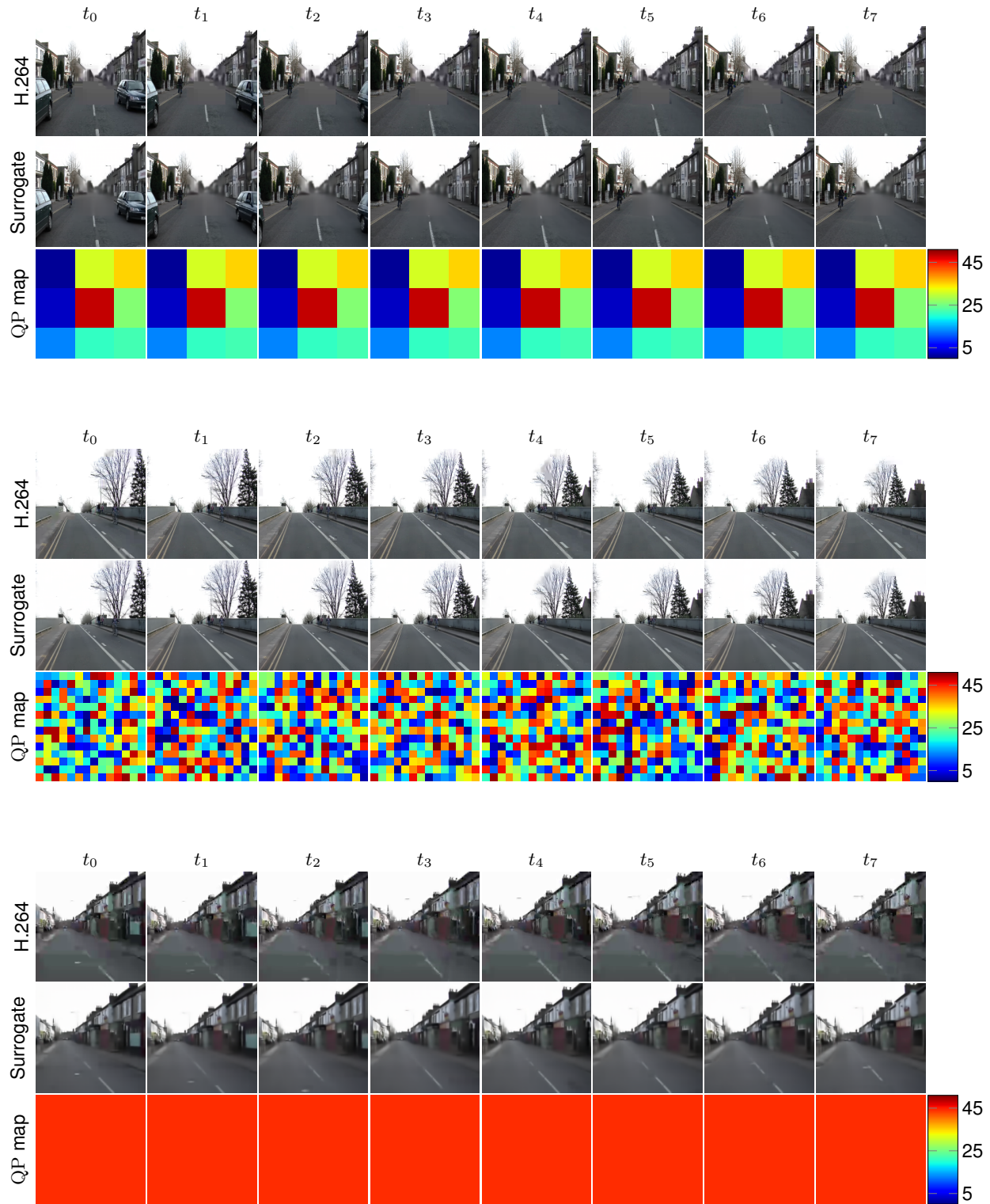


Figure 21. Qualitative surrogate model results. The first row shows the H.264 coded clip, the middle row shows the prediction of our conditional surrogate model, and the bottom row shows the macroblock-wise QP map. QP sampled over the full range. CamVid dataset used.

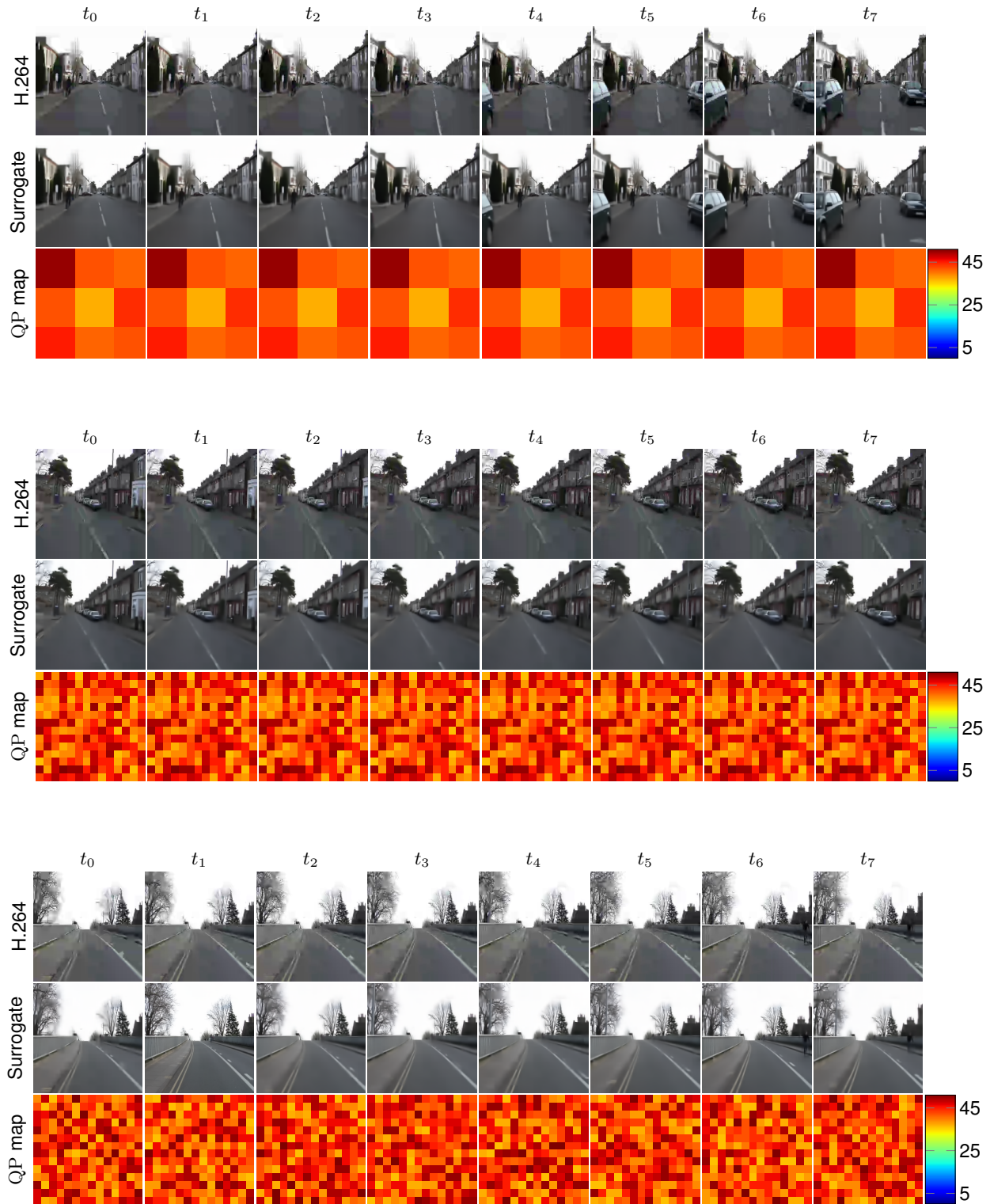


Figure 22. Qualitative surrogate model results. The first row shows the H.264 coded clip, the middle row shows the prediction of our conditional surrogate model, and the bottom row shows the macroblock-wise QP map. QP sampled from a range between 36 and 51. CamVid dataset used.

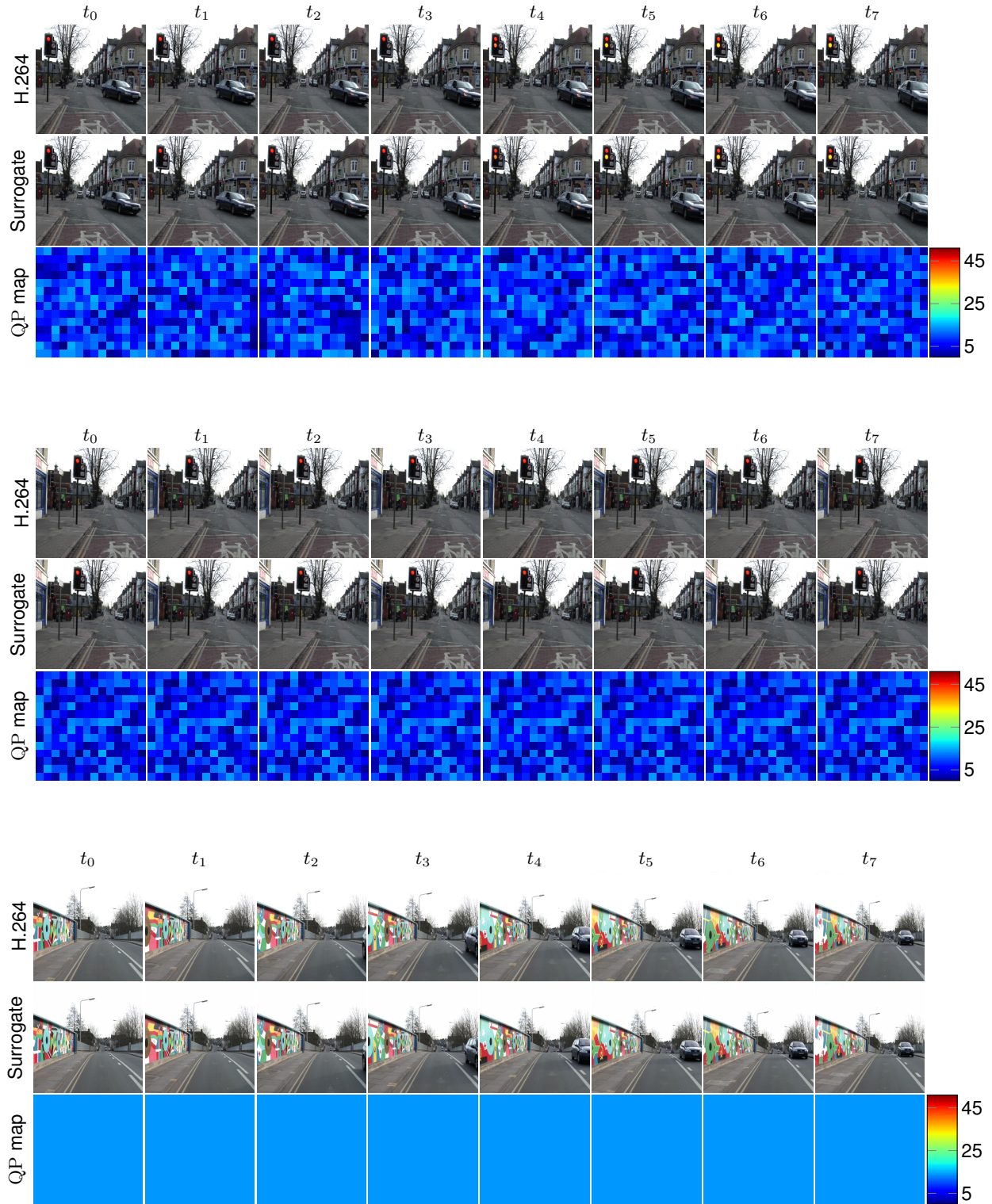


Figure 23. Qualitative surrogate model results. The first row shows the H.264 coded clip, the middle row shows the prediction of our conditional surrogate model, and the bottom row shows the macroblock-wise QP map. QP sampled from a range between 0 and 15. CamVid dataset used.

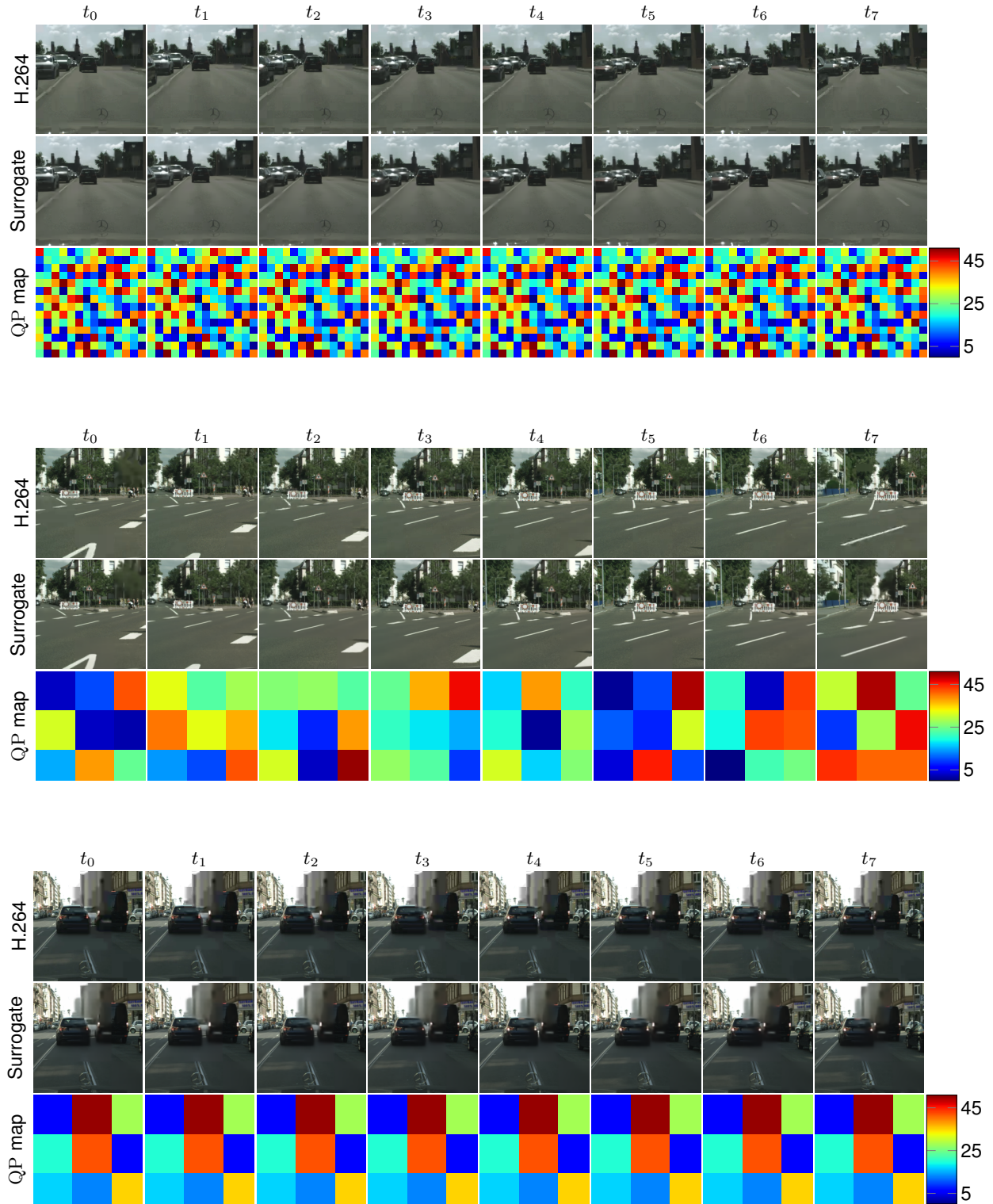


Figure 24. Qualitative surrogate model results. The first row shows the H.264 coded clip, the middle row shows the prediction of our conditional surrogate model, and the bottom row shows the macroblock-wise QP map. QP sampled over the full range. Cityscapes dataset used.

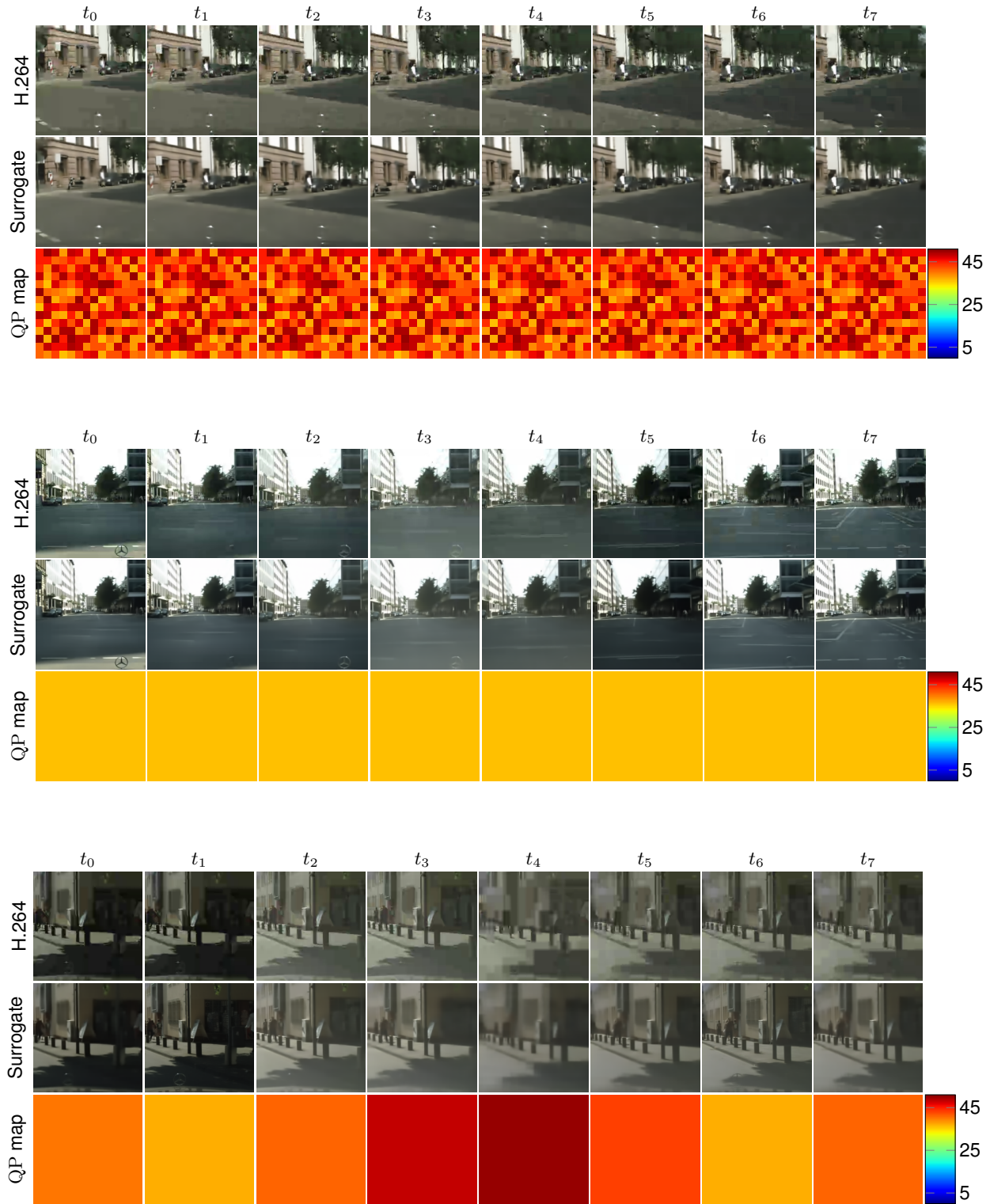


Figure 25. Qualitative surrogate model results. The first row shows the H.264 coded clip, the middle row shows the prediction of our conditional surrogate model, and the bottom row shows the macroblock-wise QP map. QP sampled from a range between 36 and 51. Cityscapes dataset used.

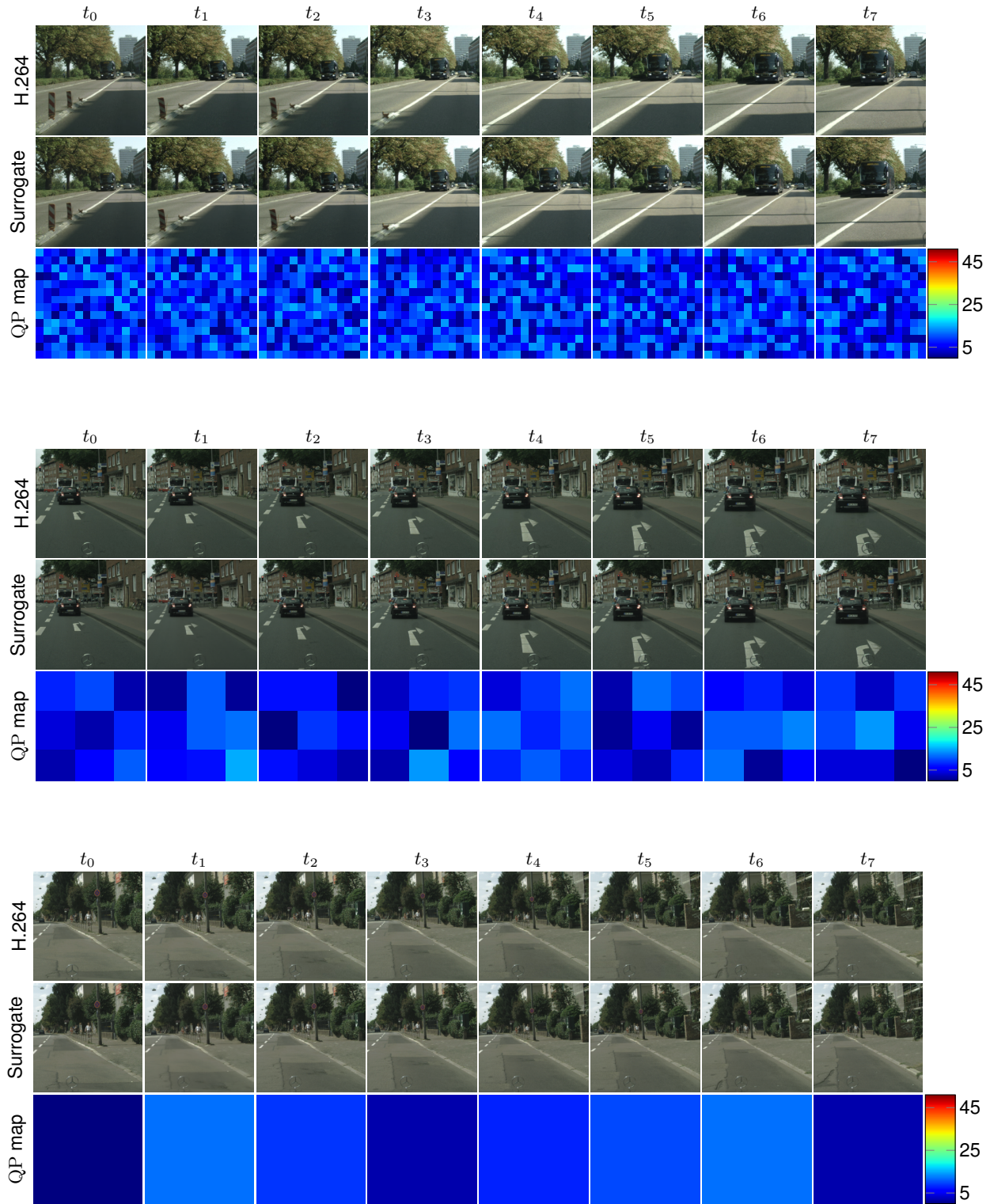


Figure 26. Qualitative surrogate model results. The first row shows the H.264 coded clip, the middle row shows the prediction of our conditional surrogate model, and the bottom row shows the macroblock-wise QP map. QP sampled from a range between 0 and 15. Cityscapes dataset used.